SAN ONOFRE NUCLEAR GENERATING STATION
UNIT 1

MASONRY WALL EVALUATION

RESPONSE TO NRC REVIEW

APPENDIX A : TECHNICAL QUESTIONS

Prepared for:

BECHTEL POWER CORPORATION
Los Angeles, California

Prepared by:

COMPUTECH ENGINEERING SERVICES, INC.
Berkeley, California

April, 1982.

TABLE OF CONTENTS

1 INTRODUCTION

In an enclosure to a letter of February 17, 1982, Docket No. 50-206 LS05-82-02-068, the NRC provided an evaluation of the non-linear inelastic time history analysis methodology for the San Onofre, Unit 1 masonry wall assessment. This evaluation included a list of technical questions and/or comments applicable to the proposed methodology.

The information in this report is provided in response to these questions. This information is supplemental to the information provided in Volumes 1, 2 and 3 of Report No. R543.02, entitled "Seismic Evaluation of Reinforced Concrete Masonry Walls".

Following this introduction a brief review of salient points of the methodology is presented. The questions from the NRC are addressed on an individual basis in successive sections and conclusions are then presented.

2 REVIEW OF ANALYSIS METHODOLOGY

The methodology for the masonry wall evaluation at the San Onofre. Unit 1 plant was based on the following properties of the walls:

a. Masonry units were reinforced both vertically and horizontally

b. Vertical and horizontal reinforcement was grouted in the walls

c. Vertical reinforcment was dowelled into foundations at the base.

d. Vertical reinforcment was anchored into well reinforced bond beams at the top.

e. Walls were well anchored to other components of the structural system.

Under these conditions the centrally located vertical reinforcment provides a ductile mechanism for out-of-plane loads that cause internal forces to exceed the elastic limit of the wall. The methodology that was developed takes into account this ductile capability.

The procedures used in the methodology were based on a formulation of the simple equilibrium balance between the reinforcing steel and the masonry face shell. Consideration of this equilibrium balance based on basic engineering mechanics led to a relatively simple model which could be coded on existing, well-tested non-linear computer programs. Once coded the model was capable of predicting reasonably well the actual load-deflection behavior of masonry walls observed in experimental tests.

The modelling of any structure or component for dynamic analysis requires consideration of three main factors:

a. Modelling of the physical structure

b. Determination of the loading function

c. Selection of solution techniques.

The seismic loading function is provided by the use of recorded ground accelerations scaled to envelope the 0.67g Housner spectrum. Solution techniques

for non-linear dynamic problems have been available for some time and have been well tested and verified. Therefore the main effort in the development of the methodology was in the physical modelling of the masonry walls. In general the model was developed from engineering mechanics principles and test results were used to validate some of the assumptions made.

3 ITEM 4(a) MASONRY FACE SHELL STRESSES

QUESTION:

> "During the entire analysis, the masonry face shell is assumed to remain elastic. There is a likelihood that the compressive stress at the face shell may exceed the f'm value and spalling of the face may occur. There is no grout core to stabilize this situation. This aspect needs thorough investigation in terms of the strength of the masonry, strain/stress magnitudes at face shell, and actual masonry block behavior during shaking."

RESPONSE:

In the following sections this item is addressed in terms of experimental data on the stress-strain relationship for plain concrete and basic engineering mechanics principles for the deformation of sections under flexure.

From a series of basic assumptions a methodology is derived for the face shell stress-strain distribution under out-of-plane loads. Ultimate strain limits in the extreme fiber are obtained from the results of published data. The methodology is then used to assess the stress distribution in the face shells of the walls at San Onofre, Unit 1. The effect of variations in some of the parameters is included in the assessment.

The stresses at this stage are derived for purely out-of-plane loading. In Section 9 of this response the impact of this face shell compression on the capability of the wall to withstand simultaneous in-plane loading is assessed.

3.1 Masonry Wall Behavior

A number of basic approximations may be made about the real behavior of masonry walls under out-of-plane non-linear loadings. These are based on engineering mechanics principles and on the results of test data.

1. In its most simplified form the wall deflects as two rigid blocks, as shown in Figure 3.1, with a central concentrated plastic hinge. The plastic hinge rotation may be obtained from geometry as:

$$\theta pl = 2\,\Delta p/(L/2)$$
$$= 4\,\Delta p/L$$

where $\Delta p = (\Delta u - \Delta y)$, i.e. plastic displacement

Total ultimate displacement is then obtained by the sum of this plastic rotation plus the yield rotation, obtained as the area of the bending moment diagram at yield over the plastic hinge length.

2. The stress-strain curve of the masonry may be idealized as a bi-linear formulation, as shown in Figure 3.2. The slopes of the two lines, Em and E'm may be expressed as a function of the masonry strength, f'm, and bounds on these slopes are obtainable from test data.

3. The masonry face shells on the compression side have a linear strain distribution over the length of bearing, as shown on Figure 3.3.

4. Plastic rotation is confined to the length of the plastic hinge, which in this formulation is considered to be equal to the length of yielding rebar. Over this length the curvature is assumed to be uniform.

3.2 Methodology

For out-of-plane loading there will be a variation of compression over the face shell area. In the following sections these non-uniform stresses due to out of plane loads are investigated.

Consider the area of face shell in contact, as shown in Figure 3.4. There are 2 unknowns:

εc = maximum outer fiber strain
b = contact length

From assumption 4 in the previous section, the curvature may be obtained from the plastic rotation and plastic hinge length as:

$$\varepsilon_c = \theta u/Lp, \text{ assumed uniform.}$$

also the curvature may be expressed as:

$$\psi_c = \varepsilon_{c/b}$$

therefore

$$\theta u/Lp = \varepsilon_{c/b}$$

$$\varepsilon_c = b\theta u/Lp \quad \ldots\ldots\ldots\ldots\ldots\ldots\ldots\ldots (3\text{-}1)$$

The total force on the face shell is also known from

$$C = T$$

where C is the total compression and T is the force in the rebar at yield stress.

Therefore assumption 2 may be used to determine the stress distribution and hence the force in the face shell in terms of ε_c and b.

Using this relationship with equation (3-1) the strain ε_c and bearing length b may be determined.

Two formulations must be considered:

1. Extreme fiber strain less than the strain at f'm. In this case the stress distribution is linear.

2. Extreme fiber strain greater than the yield strain, where the masonry stress is non-linear.

3.2.1 Linear Stress Distribution

Figure 3.5 (a) shows the strain and stress distributions in the face shell. The total compressive force is:

$$C = fcb/2$$

and from Equation (3-1)

$$b = \varepsilon_{cLp}/\theta_u$$

From assumption 1.

$$f_c = E_m \varepsilon_c$$

therefore

$$C = (E_m \varepsilon_c)(\varepsilon_{cLp})/(2\theta_u)$$

$$\varepsilon_c = \sqrt{(2C\theta_u)/(E_m L_p)} \quad \ldots\ldots\ldots\ldots\ldots\ldots (3\text{-}2)$$

3.2.2 Non-Linear Stress Distribution

For the case where the extreme fiber strain exceeds the masonry yield strain, the strain and stress distributions are as shown in Figure 3.5 (b).

From Equation (3-1) the extreme fiber strain is

$$\varepsilon_c = b\theta_u/L_p$$

and from section geometry.

$$\varepsilon'_m = b'\theta_u/L_p$$

The total compression on the section may be formulated in terms of stresses as:

$$C = (f'_m b'/2) + ((f_c + f'_m)/2)(b - b')$$

substituting

$$b = \varepsilon_{cLp}/\theta_u$$

and $$b' = \varepsilon'_{mLp}/\theta_u$$

this becomes

$$C = \frac{f'_m \varepsilon'_m L_p}{2\theta_u} + \frac{(f'_c + f'_m)(\varepsilon_c - \varepsilon'_m)}{2} \frac{L_p}{\theta_u} \quad \ldots\ldots\ldots\ldots (3\text{-}3)$$

and from assumption 2 (Figure 3.2)

$$f_c = f'_m + E'_m(\varepsilon_c - \varepsilon'_m) \quad \ldots\ldots\ldots\ldots\ldots\ldots\ldots\ldots\ldots\ldots \quad (3\text{-}4)$$

substituting (3-4) into (3-3),

$$\frac{2C\Theta_u}{L_p} = f'_m\varepsilon'_m + (2f'_m + E'_m(\varepsilon_c - \varepsilon'_m))(\varepsilon_c - \varepsilon'_m)$$

rearrange,

$$\frac{2C\Theta_u}{L_p} = -f'_m\varepsilon'_m + 2f'_m\varepsilon_c + E'_m(\varepsilon_c^2 - 2\varepsilon'_m\varepsilon_c + \varepsilon'^2_m)$$

solve for ε_c.

$$\varepsilon_c = \frac{-(2f'_m - 2E'_m\varepsilon'_m) \pm \sqrt{(2f'_m - 2E'_m\varepsilon'_m)^2 - 4E'_m(E'_m(E'_m\varepsilon'^2_m - 2C\Theta_u/L_p - f'_m\varepsilon'_m)}}{2\,E'_m}$$

$$\ldots\ldots\ldots\ldots\ldots\ldots \quad (3\text{-}5)$$

3.3 Stress/Strain Limits

There is no available test data on the shape of the falling branch of the stress strain curve for masonry face shells. A stiff testing machine is required to trace the full extent of the descending branch of the stress strain curve and this has not yet been done for masonry. Consequently the stress strain relationship of plain unconfined concrete was used to define the falling branch.

The form of the stress strain curve for plain concrete is similar to that shown in Figure 3.6(a), from Hognestad [3.1]. Ultimate strength design moment capacity is based on an extreme fiber strain of 0.003. Test results show this to be conservative [3.2]. At this strain level the compressed concrete in a flexural member will not show any visible cracking or spalling even though the strain is greater than that corresponding to maximum stress [3.4]. Blume, Newmark and Corning [3.3] recommend that an extreme fiber strain of 0.004 be used for computations of ultimate curvature involving unconfined concrete.

Because of the similarity of unconfined concrete and the face shell of the

concrete masonry blocks this limiting strain value of 0.004 has been adopted for this evaluation. Note that the ultimate strain limits from Appendix C of ACI-349, used in the computation of rotational ductility in Section 6 of this report, are considerably greater than this value of 0.004, ranging from 0.007 to 0.012. Therefore the value of 0.004 may be considered conservative relative to the ACI-349 ultimate strain capacities.

The form of the stress strain curve shown in Figure 3.6(a) has been adopted to determine ultimate strains in the San Onofre, Unit 1 masonry walls with the modifications shown in Figure 3.6(b), which are made both for compatibility with the known masonry properties and for simplifying computations:

a. The maximum stress f''c in Figure 3.6(a) is replaced with the specified minimum compressive strength, f'm.

b. The parabolic shape to maximum stress levels is replaced by a straight line with the same average slope, 2f'm/Em.

c. The elastic modulus, Em, is assumed to be 1000f'm, giving a strain of 0.002 at maximum stress.

d. The slope of the descending branch of the curve is computed as 0.15f'm/(0.002-0.0038) = -83.33f'm.

These values have been used to define stress strain parameters for use in the equations developed in the previous section. Based on these equations the ultimate strain and stress values for each of the San Onofre, Unit 1 masonry walls included in the evaluation have been computed. These are discussed in the following section. The effect of variations in the parameters defining the stress strain curve are also investigated and presented in Section 3.5.

3.4 San Onofre, Unit 1 Wall Stresses

The face shell strains and stresses for the San Onofre, Unit 1 masonry walls are summarized in Table 3.1. For each wall the extreme fiber stress and strain are listed, together with the maximum stress. For ultimate strains less than 0.002 the maximum stress occurs at the extreme fiber. For strain levels greater than 0.002 the maximum stress occurs between the extreme fiber and the neutral axis. The bearing width or distance from the extreme

fiber to the neutral axis is also tabulated for each wall.

The maximum strain in all cases is less than the limit of 0.004. Only two walls, TB-9 and TB-10, have strains greater than 0.003. In all of the Reactor Auxiliary building walls the stress in the face shell is linear as the maximum strain level does not exceed 0.002. For all the remaining walls the strain levels are such that the extreme fiber stress is less than the maximum value.

3.5 SEAOSC Test Stresses

During 1980 and 1981 the Structural Engineers' Association of Southern California (SEAOSC) carried out load tests on a series of 30 wall panels constructed of reinforced concrete, reinforced concrete masonry and reinforced brick. The 24'-0" tall test specimens were loaded monotonically using an air bag to deflection levels reaching 18" at the wall mid-height. Details of the tests and the results obtained are given in References 3.5 and 3.6.

The procedures used to determine the masonry face shell stresses and strains for the San Onofre, Unit 1 masonry walls have also been applied to the concrete masonry walls included in the SEAOSC tests. The SEAOSC tests showed that no spalling of the face shell occurred at the displacements that were recorded during the tests. The compressive stresses obtained analytically from the SEAOSC tests are listed in Table 3.2.

The stresses were first computed for the same plastic hinge length used in the wall evaluation, i.e. Lp = 18". However examination of the deflected shapes recorded over the wall height indicated that the hinge length was considerably longer, about 57". Therefore stresses were also computed for this length and for one intermediate value, 35". These results are also tabulated in Table 3.2.

The strains at the extreme fiber are very large for an Lp = 18", and far greater than would be required to cause spalling. This confirms that the actual hinge length was much longer than 18". If a hinge length of 57" is assumed from the deflected shape of the SEAOSC tests then maximum strains ranging from 0.00162 to 0.00346 are obtained. These values are similar to those obtained for the San Onofre, Unit 1 masonry walls when Lp is assumed to be only 18".

The levels of compression in the SEAOSC test specimens are much higher than for the San Onofre, Unit 1 masonry walls due to the higher steel ratio and higher steel yield strength.

Although definitive conclusions cannot be drawn from these test results they indicate that spalling does not occur at the stress, strain and deflection levels given in Table 3.2. Since these values are greater than the levels obtained in the San Onofre, Unit 1 masonry walls this is additional evidence that the face shells are capable of accomodating the maximum strains.

3.6 Variations in Stress/Strain Parameters

The effect of variations in the following parameters was studied by computing the face shell stress/strain distributions in a 20'-8" wall with an effective central deflection of 9" and reinforcing of #5 at 32":

a. Masonry specified strength, f'm was varied from 1350 to 2150 psi because test results almost invariably produce actual capacities greater than the specified minimum. This is a variation of +60%.

b. The steel strength was varied to allow for a possible overstrength of up to +12.5% (5 ksi). This was achieved by varying the face shell compressive force, which is directly proportional to the steel strength.

c. The slope of the first, elastic curve (Em/2) on the masonry stress strain curve was varied by +/-20%, i.e. from 400f'm to 600f'm.

d. The second falling slope of the masonry stress strain curve was varied by +/-20%, i.e. from -100f'm to -66.68f'm.

e. The effective plastic hinge length was varied from 18" to 42".

The results of these parameter studies are summarized in Table 3.3 and the results presented graphically in Figures 3.7 to 3.11. In these figures, the face shell stress distribution is plotted above the horizontal axis and the strain below the horizontal axis. Each plot shows the effect of variation of one of the parameters listed above. A summary of these effects is as

follows:

a. An increase in the masonry strength causes an increase in the extreme fiber stress but a decrease in the maximum strain levels. The 60% increase in f'm produced a decrease in ultimate strain of about 30% and a similar reduction in the width of face shell in bearing.

b. The increase in the steel yield strength, Fy, and the corresponding increase in total compression force on the face shell had a relatively small effect on the face shell. A 12.5% increase in Fy produced a 10% increase in the extreme fiber strain. Note that such an increase in steel yield strength would reduce the deflections and thus the plastic rotation and ultimate strain. Therefore the effects would actually be less than computed in this section.

c. The maximum strain increased in inverse proportion to the first slope of the masonry stress strain curve. A 20% decrease in Em produced a 6% strain increase and a 20% increase produced a 4% reduction.

d. The results proved insensitive to a change in slope of the falling branch of the masonry stress strain curve of +/- 20%.

e. Maximum strains decreased markedly for an increase in the length of the plastic hinge. For a length of 42", less than the apparent hinge length from the SEAOSC tests, the extreme fiber strain was less than 0.002 and thus the stress distribution was linear.

3.7 Summary

A number of basic approximations enabled a formulation for the stress and strain in the masonry face shell to be derived. Consideration of experimental data on unconfined concrete provided a proposed limit of 0.004 on the ultimate strain in the extreme fiber. The computed strains in all walls were less than this value and in all but two walls were less than 0.003.

The results of the SEAOSC tests were processed to provide face shell stresses and strains using the same formulation. If the plastic hinge length of 57" inferred from the deflected shapes was used the maximum strain in the test walls was 0.00346. This is the same order as the maximum value obtained from the San Onofre, Unit 1 masonry walls and provides experimental evidence that no face shell spalling occurs at these levels.

A series of parametric studies has shown that the assumed ranges of uncertainty in a number of parameters would not be sufficient to significantly change the evaluation of the walls.

3.8 References

[3.1] E. Hognestad, "A Study of Combined Bending and Axial Load in Reinforced Concrete Members", University of Illinois, Engineering Experimental Station, Bulletin Series No. 399, November, 1951.

[3.2] A. H. Mattock, L. B. Kriz and E. Hognestad, "Rectangular Concrete Stress Distribution in Ultimate Strength Design", Journal ACI, Vol. 57, No. 8, February, 1961.

[3.3] J. A. Blume, N. M. Newmark and L. H. Corning, "Design of Multistory Reinforced Concrete Buildings for Earthquake Motions", Portland Cement Association, Chicago, 1961.

[3.4] R. Park and T. Paulay, "Reinforced Concrete Structures", John Wiley and Sons, 1975.

[3.5] Selna, L. G., "Slender Wall Tests Instrumentation and Results", Proceedings, SEAOC Annual Convention, San Diego. September, 1981.

[3.6] Foth, U. A., and Johnson, J. R., "Results of Slender Wall Tests", Proceedings, SEAOC Annual Convention, San Diego. September, 1981.

BUILDING	WALL I.D.	EXTREME FIBER		MAXIMUM STRESS	BEARING WIDTH
		STRESS	STRAIN		
TURBINE	TB-1a	1244	0.00295	1350	0.442
	TB-1b	1311	0.00235	1350	0.501
	TB-2	1310	0.00236	1350	0.500
	TB-3	1310	0.00236	1350	0.500
	TB-4	1310	0.00236	1350	0.500
	TB-5	1244	0.00295	1350	0.442
	TB-6	1244	0.00295	1350	0.442
	TB-7a	1244	0.00295	1350	0.442
	TB-7b	1310	0.00236	1350	0.500
	TB-8	1311	0.00235	1350	0.501
	TB-9	1178	0.00353	1350	0.416
	TB-10	1178	0.00353	1350	0.416
	TB-11	1244	0.00295	1350	0.442
	TB-12	1244	0.00294	1350	0.592
VENTILATION	VB-1	1288	0.00255	1350	0.921
	VB-2	1288	0.00255	1350	0.921
	VB-3	1288	0.00255	1350	0.921
	VB-4	1288	0.00255	1350	0.921
REACTOR AUXILIARY	SB-1	878	0.00130	878	0.592
	SB-2	878	0.00130	878	0.592
	SB-3	878	0.00130	878	0.592
	SB-4	878	0.00130	878	0.592
	SB-5	534	0.00079	534	0.974
	SB-6	878	0.00130	878	0.592
	SB-7	878	0.00130	878	0.592

NOTES:

1. The values listed above are the maxima from the three earthquake records considered in the analysis.

TABLE 3.1 : SONGS-1 MAXIMUM STRESSES AND STRAINS

WALL #	TYPE	Lp	MAX. DISP.	EXTREME FIBER		MAXIMUM	BEARING
				STRESS	STRAIN	STRESS	WIDTH
1	10"	18	7.10	1888	0.00406	2460	0.762
	CMU	35		2254	0.00227	2460	0.829
		57		2389	0.00162	2460	0.963
2		18	8.00	1780	0.00459	2460	0.764
		35		2209	0.00250	2460	0.808
		57		2362	0.00175	2460	0.923
3		18	19.00	Cannot achieve equilibrium			
		35		1545	0.00574	2460	0.782
		57		2012	0.00346	2460	0.767
4	8"	18	11.20	1568	0.00641	2595	0.762
	CMU	35		2233	0.00333	2595	0.771
		57		2454	0.00231	2595	0.871
5		18	10.30	1696	0.00582	2595	0.752
		35		2281	0.00311	2595	0.782
		57		2480	0.00219	2595	0.896
6		18	14.80	885	0.00957	2595	0.861
		35		2031	0.00427	2595	0.747
		57		2343	0.00282	2595	0.804
7	6"	18	17.70	1318	0.00904	3185	0.680
	CMU	35		2578	0.00429	3185	0.628
		57		2941	0.00292	3185	0.697
8		18	15.90	1663	0.00774	3185	0.648
		35		2678	0.00391	3185	0.638
		57		2996	0.00272	3185	0.721
9		18	11.00	2075	0.00619	3185	0.624
		35		2934	0.00295	3185	0.694
		57		3139	0.00218	3185	0.834

TABLE 3.2 : SEAOSC TEST STRESSES

PARAMETER VARIED	VALUE OF VARIABLE	EXTREME FIBER		MAXIMUM STRESS	BEARING WIDTH
		STRESS	STRAIN		
Masonry Specified Mininum Strength	1350 psi	1193	0.00339	1350	0.421
	1550 psi	1413	0.00306	1550	0.379
	1750 psi	1632	0.00281	1750	0.349
	1950 psi	1850	0.00262	1950	0.324
	2150 psi	2067	0.00246	2150	0.305
Steel Strength	40 ksi	1193	0.00339	1350	0.421
	41 ksi	1186	0.00346	1350	0.429
	42 ksi	1178	0.00353	1350	0.438
	43 ksi	1170	0.00360	1350	0.446
	44 ksi	1163	0.00367	1350	0.455
	45 ksi	1155	0.00374	1350	0.463
Masonry Modulus (Elastic Slope)	400 f'm	1225	0.00361	1350	0.448
	450 f'm	1207	0.00349	1350	0.433
	500 f'm	1193	0.00339	1350	0.421
	550 f'm	1182	0.00331	1350	0.411
	600 f'm	1172	0.00325	1350	0.403
Masonry Modulus (Falling Slope)	-100 f'm	1160	0.00341	1350	0.423
	-91.7 f'm	1177	0.00340	1350	0.422
	-83.3 f'm	1193	0.00339	1350	0.421
	-75.0 f'm	1210	0.00338	1350	0.420
	-66.8 f'm	1226	0.00337	1350	0.418
Plastic Hinge Length, Lp	18"	1193	0.00339	1350	0.421
	24"	1265	0.00276	1350	0.456
	30"	1306	0.00239	1350	0.495
	36"	1332	0.00216	1350	0.535
	42"	1344	0.00199	1344	0.576

NOTES:

1. All studies were performed on a 20'-8" wall with an effective central deflection of 9".

TABLE 3.3 : EFFECT OF VARIABLES IN STRESS/STRAIN CURVES

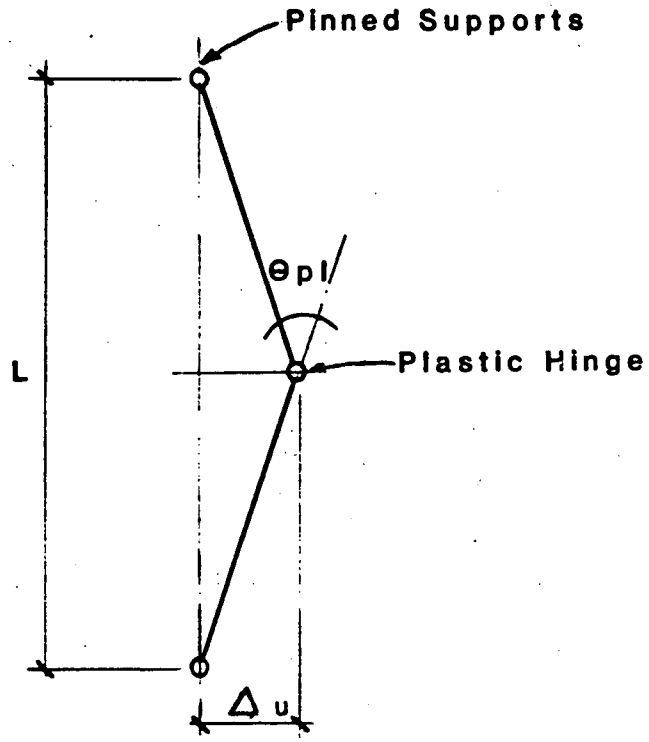

FIGURE 3.1 WALL DEFORMATION

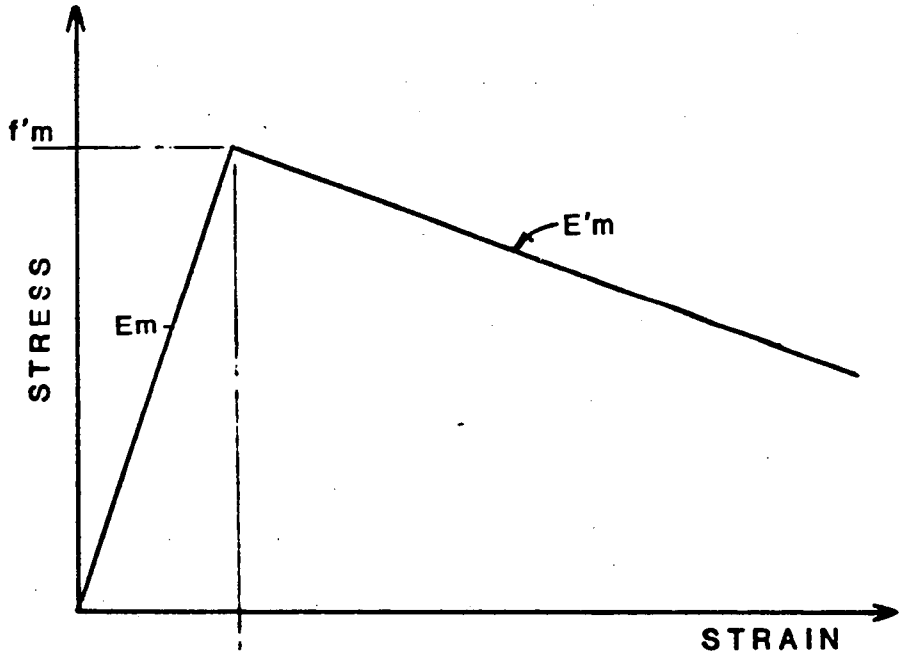

FIGURE 3.2 MASONRY STRESS-STRAIN CURVE

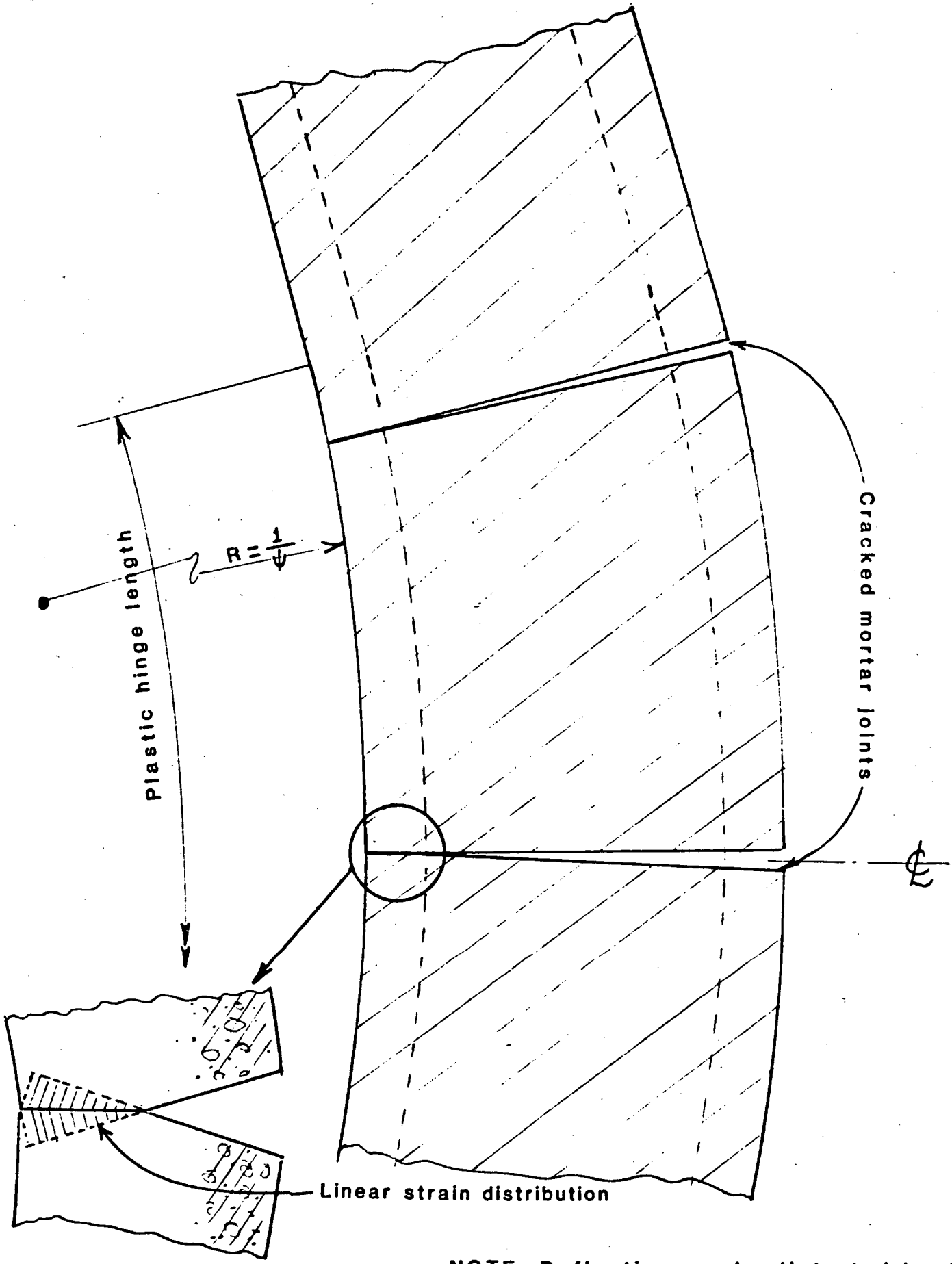

NOTE: Deflection scale distorted by 2.5

FIGURE 3.3 : CONTACT AREA OF FACE SHELL

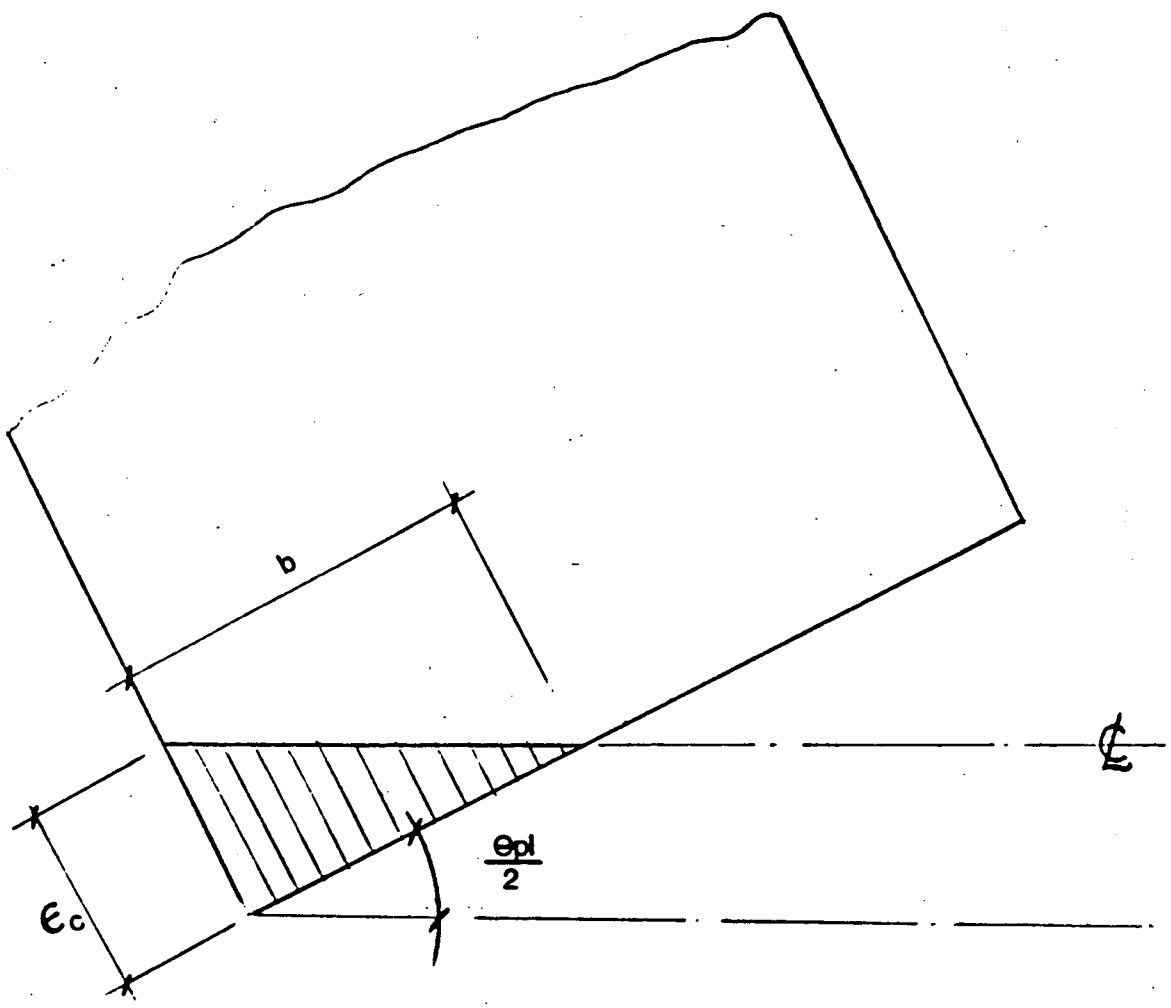

FIGURE 3.4 STRAIN DISTRIBUTION IN FACE SHELL

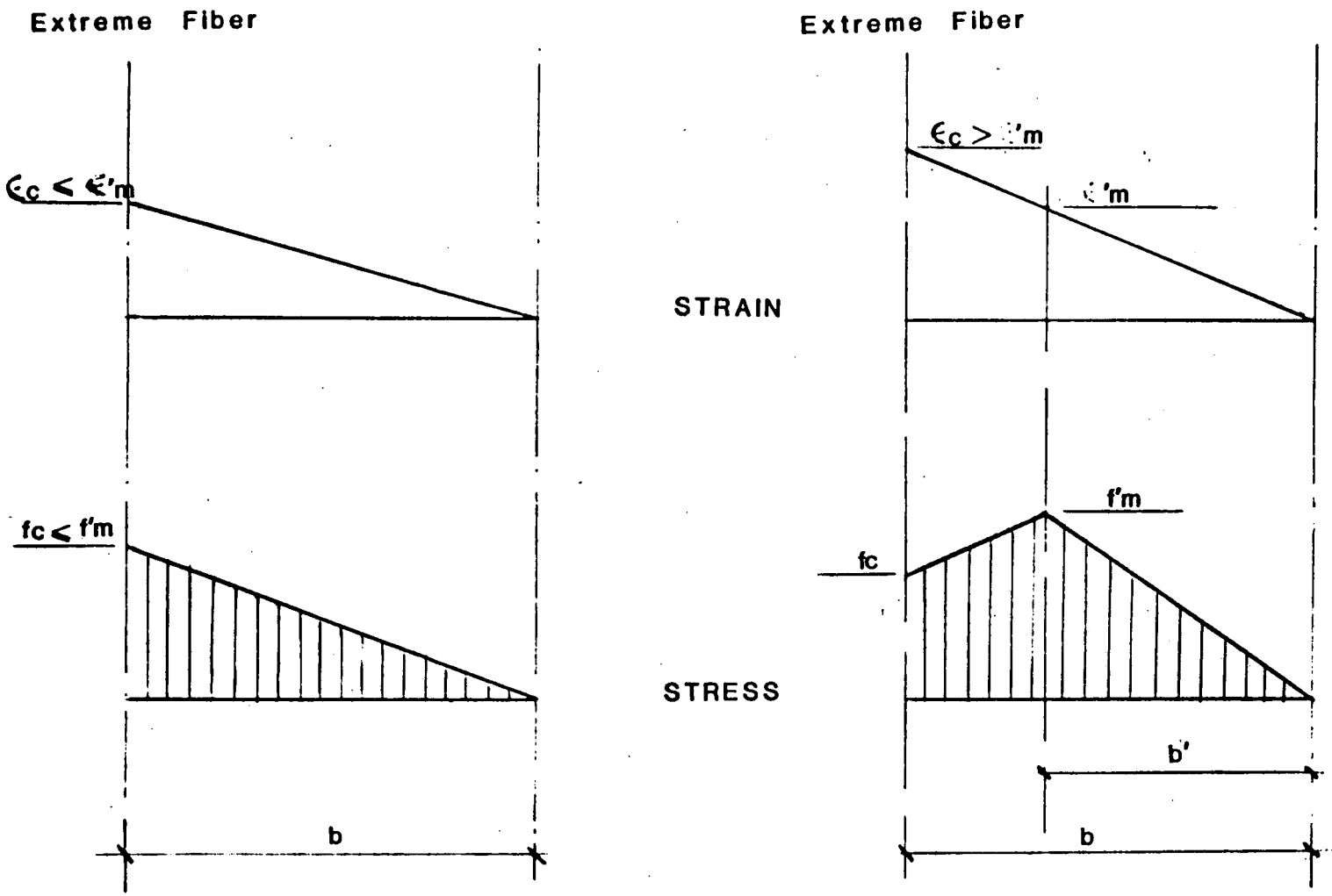

(a) LINEAR

(b)NON-LINEAR

FIGURE 3.5 STRESS-STRAIN DISTRIBUTION

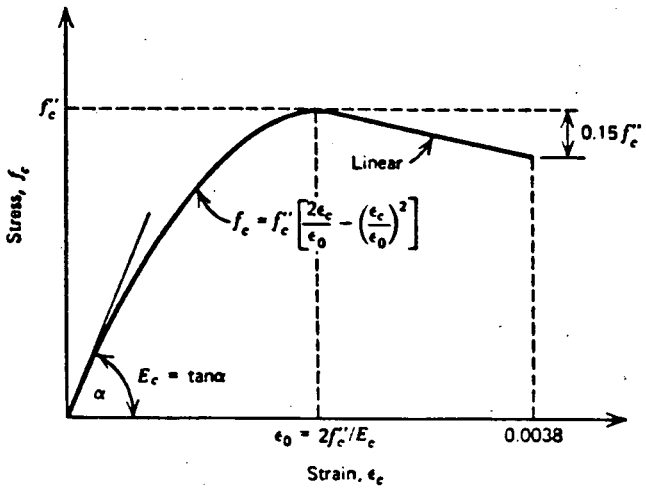

(REFERENCE 3.1)

FIGURE 3.6 (a) : IDEALIZED STRESS-STRAIN CURVE FOR CONCRETE

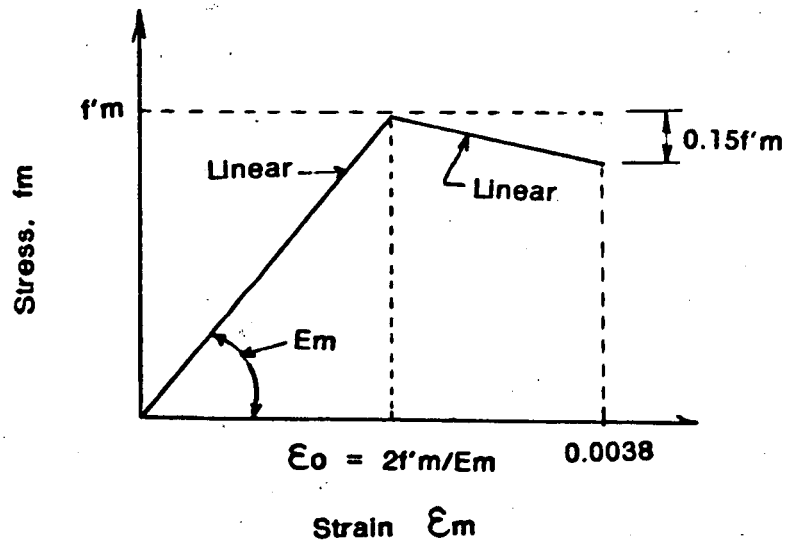

FIGURE 3.6 (b) : IDEALIZED STRESS-STRAIN CURVE FOR MASONRY

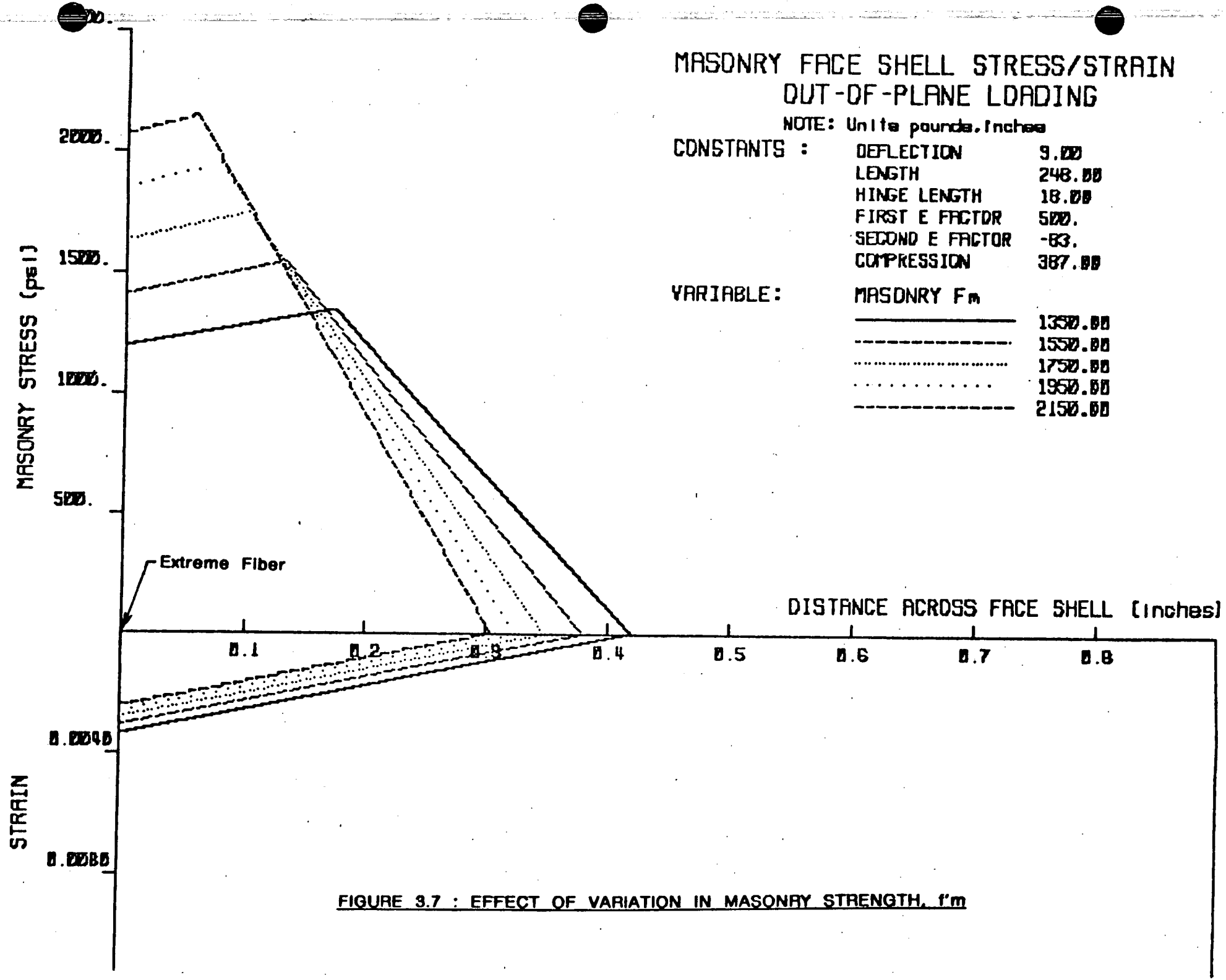

FIGURE 3.7 : EFFECT OF VARIATION IN MASONRY STRENGTH, f'm

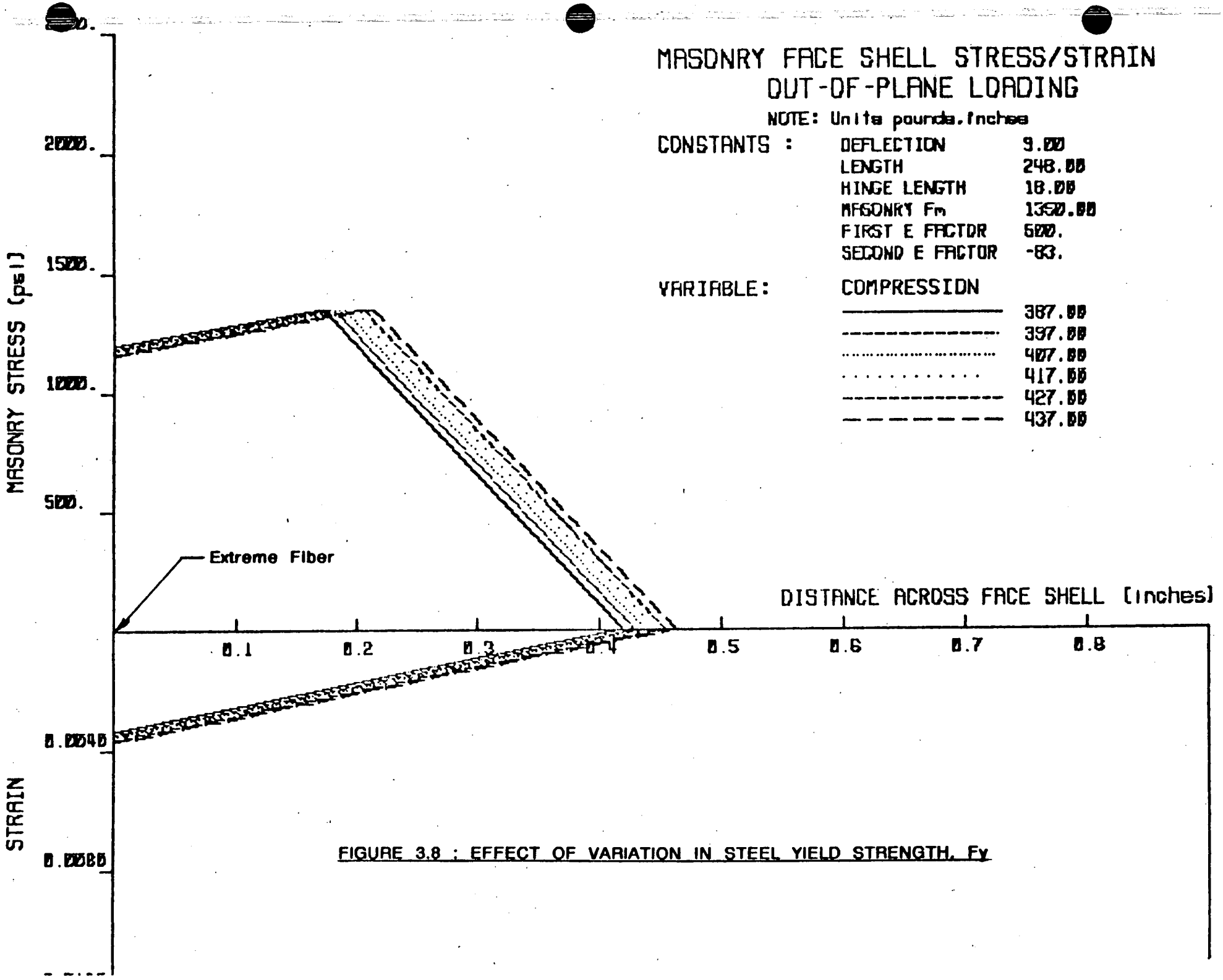

FIGURE 3.8 : EFFECT OF VARIATION IN STEEL YIELD STRENGTH, Fy

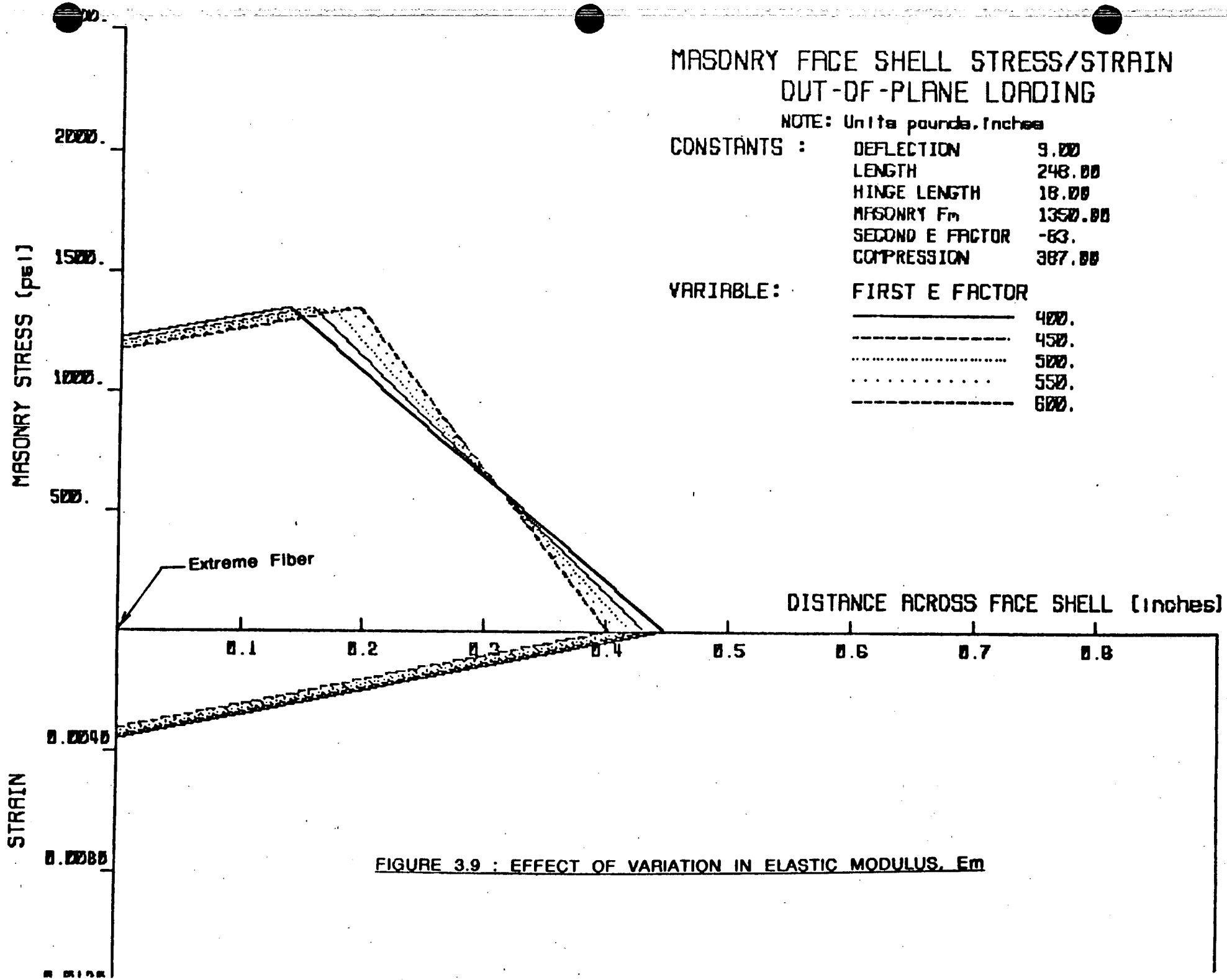

FIGURE 3.9 : EFFECT OF VARIATION IN ELASTIC MODULUS, Em

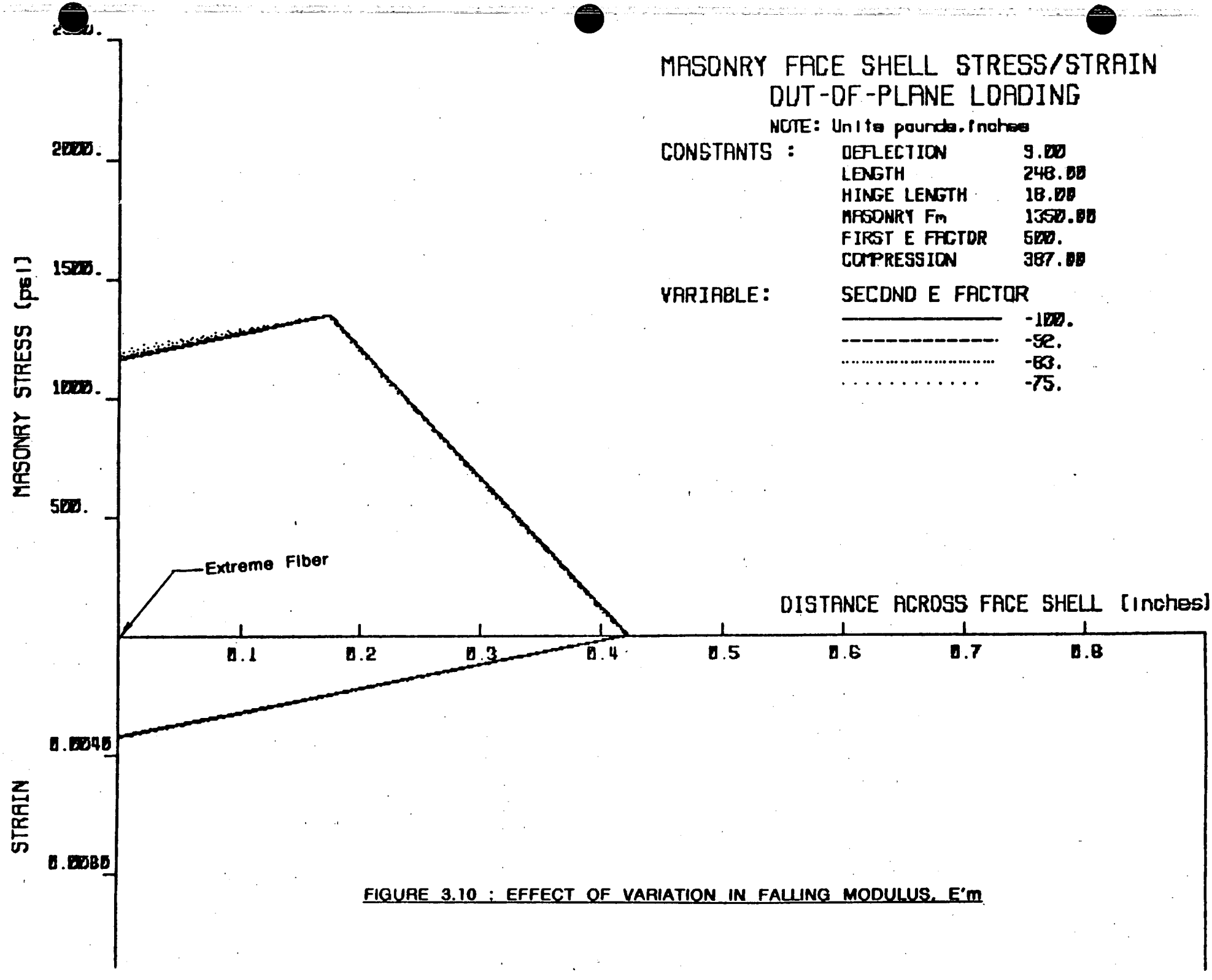

FIGURE 3.10 : EFFECT OF VARIATION IN FALLING MODULUS, E'm

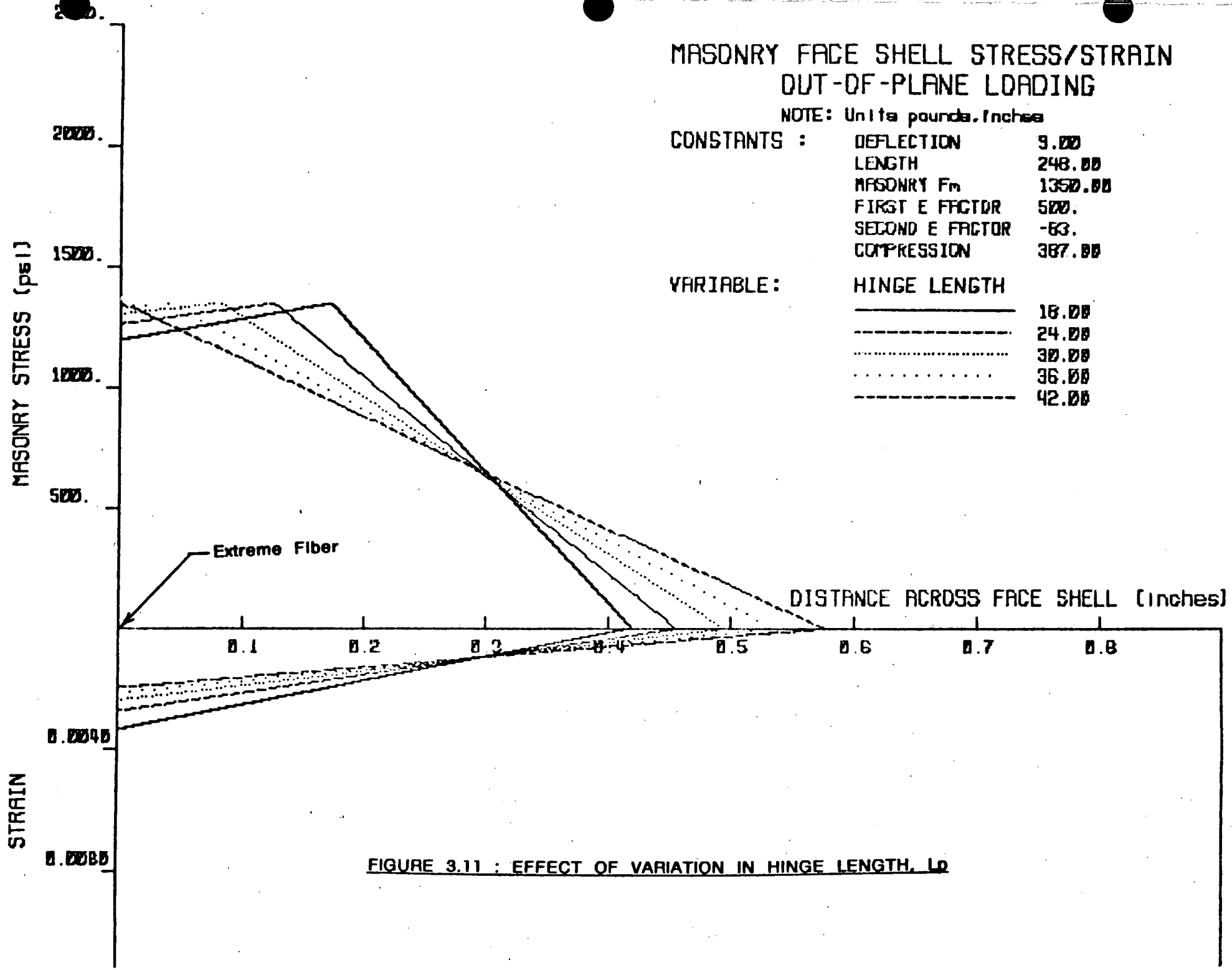

FIGURE 3.11 : EFFECT OF VARIATION IN HINGE LENGTH, Lp

4 ITEM 4(b) DAMPING SPECIFICATION

QUESTION

> "In the non-linear analysis the concept of modal and Rayleigh damping, which is applicable in the linear analysis, is used. The treatment of damping needs additional justification/ verification. In addition, the seven percent value used also needs additional verification. Considering the uncertainty in the treatment and the value of damping, at least a parametric study will be required to address the concerns in this area."

RESPONSE:

The response to this item is divided into three parts. In Section 4.1 a justification of the actual material damping used is given. Section 4.2 describes the means for implementing this damping into the model for the evaluation of the walls and in Section 4.3 the results of a number of studies to determine effective damping are presented.

4.1 Material Damping Value

For all analyses it was assumed that the viscous damping ratio for masonry was 7% of critical. This value is as specified in the BOPSSR criteria for San Onofre, Unit 1, for cracked masonry and is based on the similarity between cracked masonry and reinforced concrete. The same material mechanisms which give rise to damping apply to both materials, and damping of 7% is widely used for reinforced concrete at DBE load levels.

The design loadings for the masonry walls at San Onofre, Unit 1 are far in excess of the levels required to cause cracking and it is therefore considered to be valid to use the 7% value rather than the 4% specified in the BOPSSR criteria for uncracked masonry.

It should be noted that the value of 7% for DBE loadings is also consistent with the NRC "SEB Criteria for Safety-Related Masonry Wall Evaluation" which was provided as an enclosure with the technical questions. Section 4 (d) of these criteria specifies that "Damping values to be used for dynamic analysis shall be those for reinforced concrete given in Regulatory Guide

1.61". This referenced document provides for 7% of critical damping under DBE load levels for reinforced concrete.

4.2 Implementation in Model

The energy loss in elastic systems occurs solely through viscous damping which is proportional to velocity. In nonlinear systems an additional energy loss occurs through hysteretic material response. In nonlinear analysis this latter form of energy loss is incorporated by the use of yield functions for the inelastic materials. The viscous damping effects are included by the use of damping constants applied to the velocities.

To obtain these damping constants use is made of the uncoupled modes of the original elastic structure in the form of a Rayleigh formulation where the damping matrix is defined as:

$$[C] = a[M] + b[K]$$

where

[C] = damping matrix
[M] = mass matrix
[K] = stiffness matrix

and

a and b are damping constants.

Each of these damping constants is frequency dependent. For linearly elastic analyses the frequencies of the normal modes and thus modal damping remain constant. However when nonlinear material response occurs the concept of normal modes is not valid. The effective damping will then vary as degradation causes the frequency of the response to vary. To account for this the damping constants are selected such that the effective damping will not exceed the specified value when period elongation occurs due to material nonlinearity.

To ensure that the specified damping was not exceeded in the San Onofre, Unit 1 wall evaluation a further conservatism was introduced by specifying stiffness damping for the plane stress elements only. The gap elements modelling the face shell and the truss elements representing the rebars had hysteretic damping effects only. This is a significant conservatism as the deformations are concentrated in these joint elements and so a significant

portion of the stiffness damping has been neglected. In the following section the impact of this conservatism is assessed.

4.3 Parametric Studies

To assist in determining the effective damping in the analyses energy plots have been produced. These plots provide a graphic representation of the total energy input to a system and the components of this energy. The total energy is divided into its components of elastic strain energy, hysteretic energy, damping energy and kinetic energy. The elastic strain energy and the kinetic energy together represent the amount of energy stored by the structure. The remaining two components, damping plus hysteretic energy, are the amount of dissipated energy. The difference between the sum of the stored and dissipated energy and the total input to the system by the earthquake accelerations is the energy error. For the San Onofre, Unit 1 masonry wall evaluation the kinetic energy was zero because no static loads were applied concurrently with the earthquake loads.

Figures 4.1 to 4.4 represent the results of these studies. These time history plots are for the center displacement and the total enery calculations for two analyses of the Turbine Building Group I walls. The first two represent full elastic response, obtained by setting the yield level of the rebar very high. The second pair of plots are for the inelastic response of the same model, using the actual rebar yield level.

The particular wall used had the full added mass effects included. This gave the greatest displacement response of any wall included in the evaluation and also showed the maximum period elongation due to inelastic effects.

Because of the the difficulty of quantifying damping in an inelastic system reliance has been placed on studying the comparable response between the elastic and inelastic analyses of the same systems. From the similarities and the differences engineering judgment allows conclusions to be made about the effective damping.

The following comparisons between the two analyses may be noted:

a. Displacements for the elastic system as shown in Figure 4.1 were similar to the inelastic response of Figure 4.3 for the initial segment of the earthquake record but after several cycles

of yielding the inelastic displacements were several times the elastic values.

b. The displacement time histories illustrate clearly the divergence of the period of response of the inelastic system compared with the elastic frequency response which remains essentially constant with almost entirely first mode response.

c. The total energy represented by the upper line in the plots of Figures 4.2 and 4.4 shows the rate of energy input into the structure. After a slow buildup from zero to 1.5 seconds the steepest gradient occurs from 1.5 to 3.0 seconds representing the strongest shaking. From 3.0 to 6.0 seconds a second period of strong shaking occurs and the slope then reduces for the remainder of the analysis as the intensity decays.

d. The total energy input into both the elastic system and the yielding system is essentially the same up to a time of 6 seconds. After this period the rate of energy input to the yielding system is reduced as the period elongates.

e. At time 6.0 seconds the total input to both systems is approximately 9200 lb-in. For the elastic system 1200 lb-in of energy is stored and the remaining energy is dissipated by the total damping of 8200 lb-in. For the inelastic system slightly less energy is stored, 1000 lb-in, and of the remainder 1800 lb-in is dissipated by hysteretic behavior and 6400 lb-in by damping. Thus the elastic model dissipates 89% of the total input by damping and the inelastic model 70%. The inelastic model also dissipates 20% by non-linear material behavior.

f. At the end of the analysis, 30 seconds, the total energy to the elastic system is 19200 lb-in of which 18800 lb-in is dissipated by damping, or 98%. The inelastic system has a total energy input of 17600 lb-in, 8% less than for the equivalent elastic system. Of this total 14% is dissipated in hysteretic material response and 84% in the viscous damping mechanism. The remaining 2% is stored as elastic strain energy.

Conclusive evidence as to the exact proportion of critical damping in an

inelastic system cannot be obtained because of the complexity of the changing frequency of the system. However the results discussed above are considered to give a general validation that the method of incorporating the specified damping into the masonry wall model effectively provides conservative levels of damping. At the end of the period of strong shaking the inelastic model has dissipated considerably less energy by damping compared with the elastic analysis, 70% compared with 89%, even though up to this stage the total energy input is similar and the frequency response of both responses is similar.

At the conclusion of the portion of earthquake record analyzed, 30 seconds, essentially all the total input in the elastic system is dissipated by the specified 7% damping with only 2% stored as strain energy. For the non-linear model the damping in the model dissipates 84% of the total energy with most of the remainder dissipated as hysteretic behavior.

4.4 Summary

The specified 7% damping used for cracked reinforced concrete masonry under DBE loads has been justified in terms of the similarity of the mechanisms of material damping between reinforced masonry and reinforced concrete. This similarity has been recognized in the NRC criteria for masonry evaluation.

The method used to implement this damping in the nonlinear model has been explained in more detail and the general proportion of effective damping illustrated by comparing the total energy balance with an equivalent elastic system. The nonlinear model was demonstrated to dissipate approximately 20% less energy by viscous damping using the specified damping constants even when the total energy and frequency response of both systems was similar. Both systems stored only a small fraction of the total energy as strain energy. For the elastic response the remainder was dissipated entirely by viscous damping and for the yielding system was split between hysteretic and viscous damping.

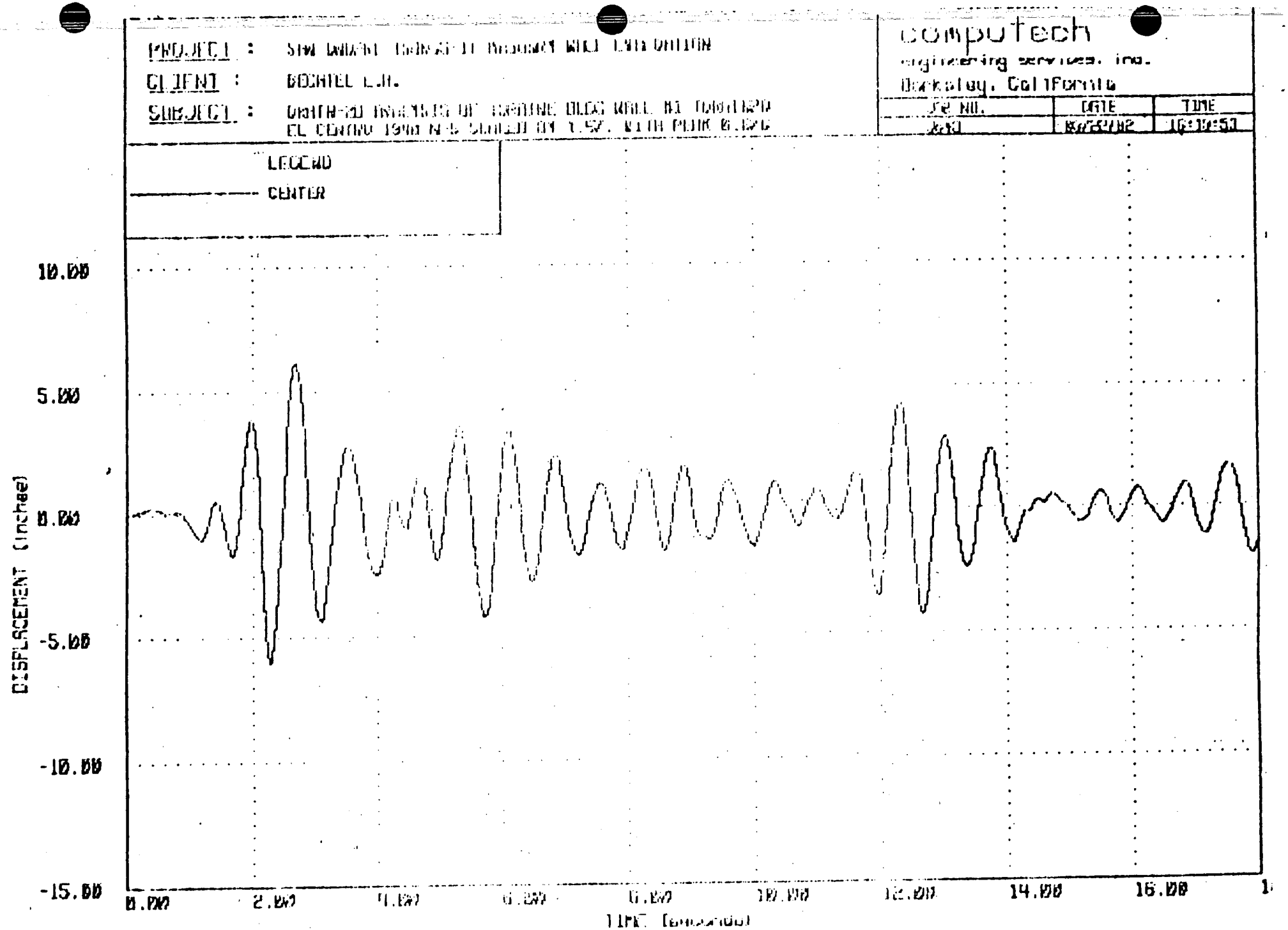

FIGURE 4.1 : DISPLACEMENT RESPONSE OF ELASTIC WALL

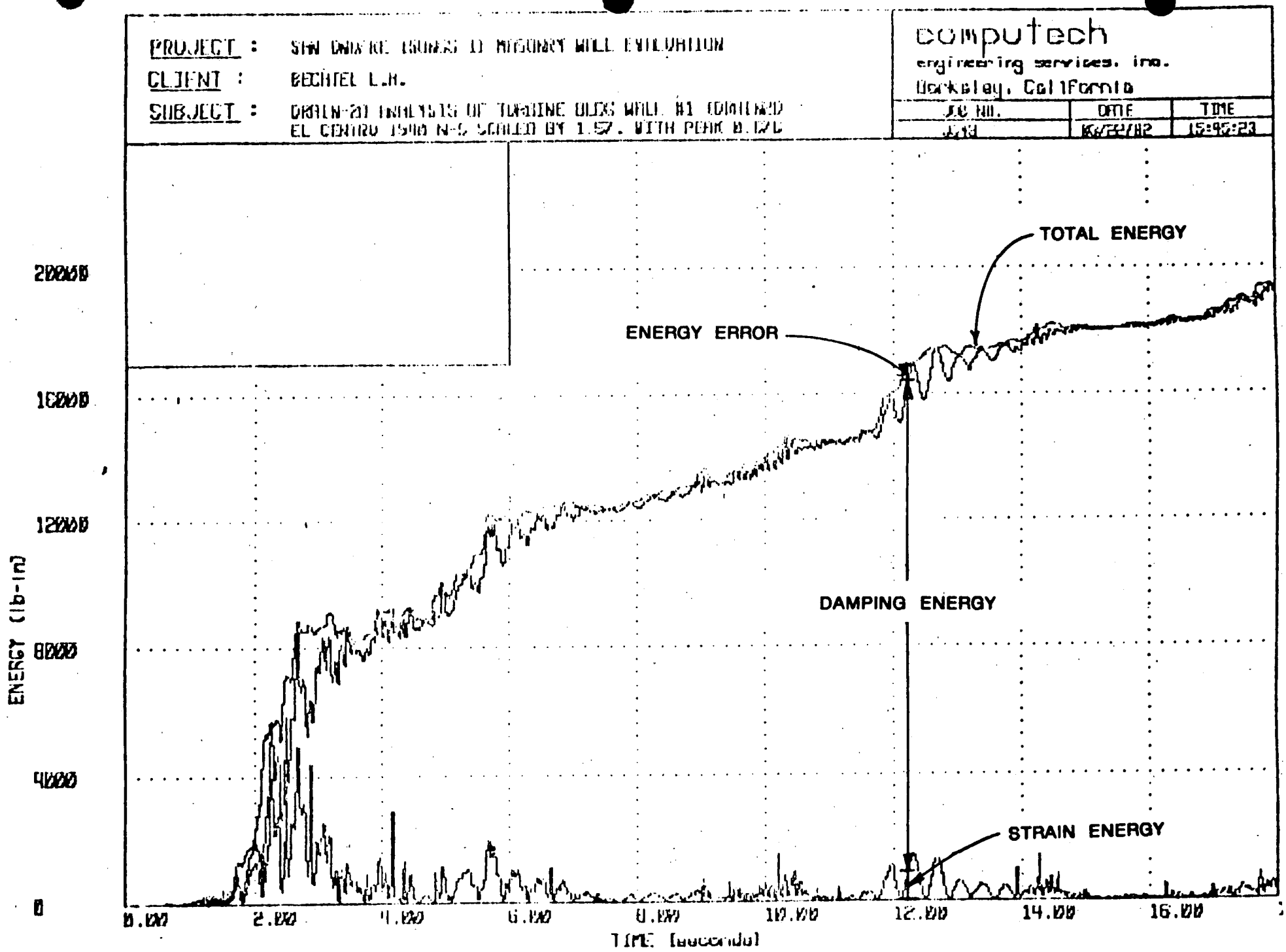

FIGURE 4.2 : ENERGY BALANCE OF ELASTIC WALL

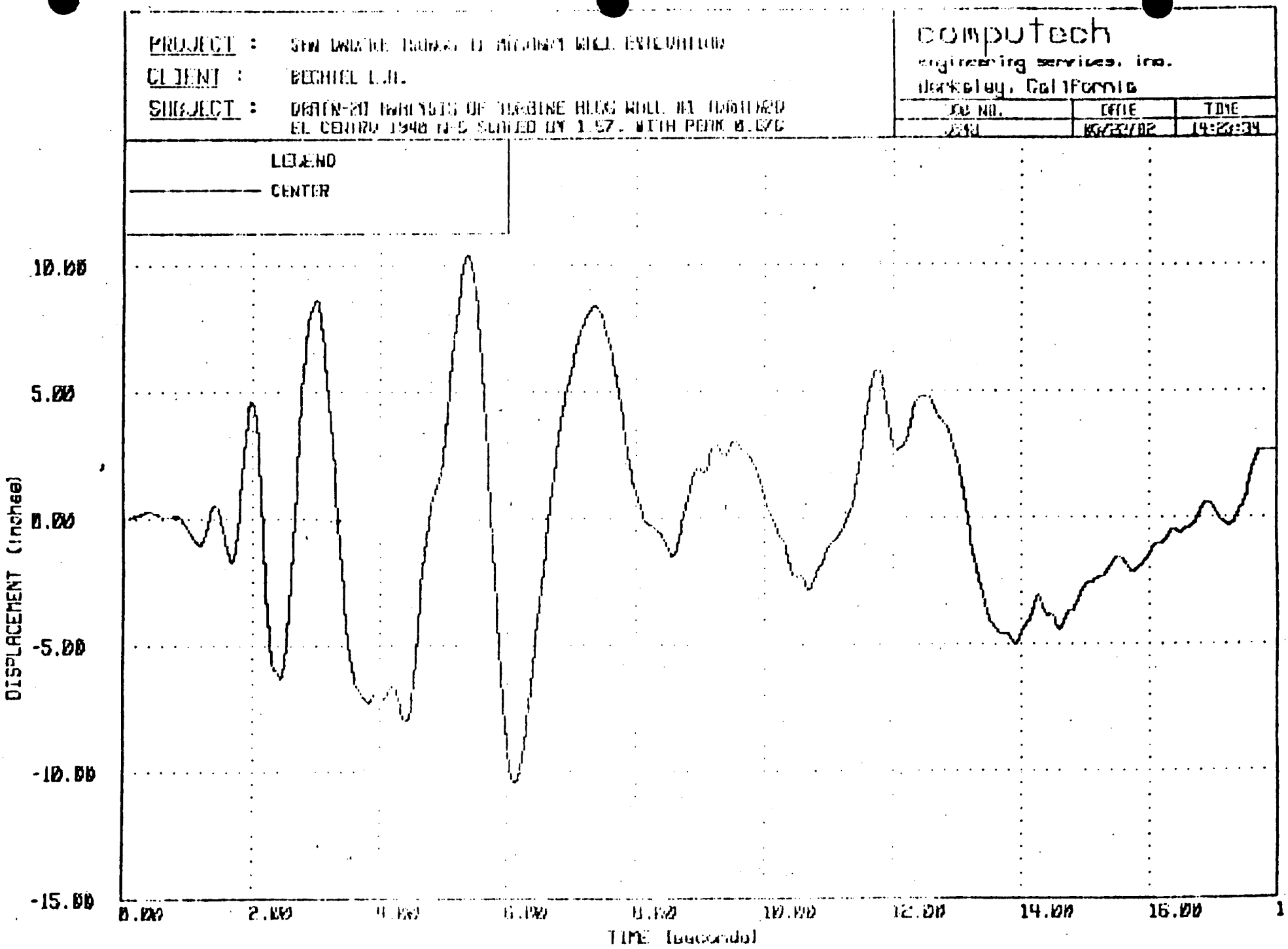

FIGURE 4.3 : DISPLACEMENT RESPONSE OF YIELDING WALL

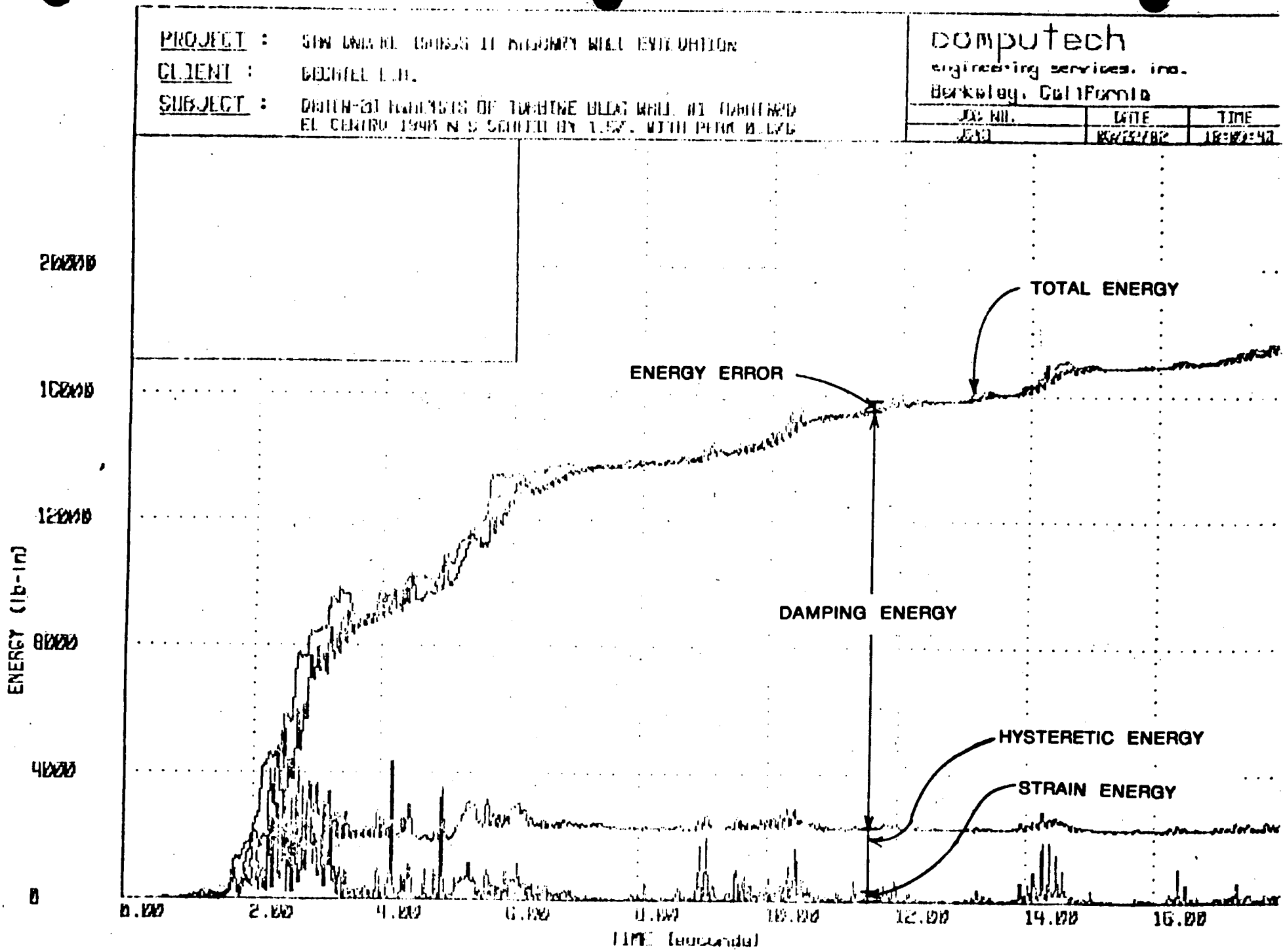

FIGURE 4.4 : ENERGY BALANCE OF YIELDING WALL

5 ITEM 4(c) REBAR LENGTH AND Ljt

QUESTION:

> "The selection of the length of rebar assumed to yield in the analysis is arbitrary. At present, there is no data to provide the basis for such selection. Also, it needs to be verified that the parameter, Ljt, related to cracked joint widths is problem independent."

RESPONSE:

Figure 5.1 shows the way in which the parameters Ljt and Lb were utilized in the inelastic masonry wall model. These two parameters, the rebar length, Lb and the assumed width of the cracked joint, Ljt, effectively define the slopes of the two lines forming the hysteresis curve for the cyclically loaded specimen. In addition the length of rebar assumed to yield, Lb, effectively defines the plastic hinge length and governs the maximum steel strain. Values for these parameters were not selected as an arbitrary choice but were based on theoretical considerations as is discussed in the response to this question.

The cracked joint width, Ljt, was expected to be an important parameter in the development of the model and figured prominently in the early series of parametric studies. However, these studies showed that the non-yielding portion of the wall could be accurately modelled using an average effective stiffness based on 1.5 times the transformed moment of inertia. Thus in the final model Ljt was not of major importance since it only contributed to the total length of yielding rebar in the hinging portion. Its use in defining the stiffness in the elastic portion was replaced by the use of 1.5 times the cracked moment of inertia.

The response to this question is divided into two parts in the following sections: Section 5.1 provides theoretical considerations for the justification of the rebar length and the effective stiffness based on Ljt. Section 5.2 presents the results of a parameter study on variations in the two parameters Lb and Ljt.

5.1 Theoretical Considerations

The effect of cracking on a section of wall under flexure is shown in Figure

5.2. The cracking will be concentrated at the mortar joints and between these joints transfer of stress by bond in the grout core will cause some tension in the uncracked masonry units. Therefore the steel stress will reduce from a maximum at the cracked joints to a minimum at the center of the masonry unit. The effective stiffness, EI, will vary inversely to the steel stress.

This behavior defines the effective stiffness of a partially cracked wall. As the moments increase the steel stress distribution may be used to track the spread of the hinging portion of the wall. This is discussed further in the following sections as it effects the parameters Lb and Ljt.

5.1.1 Yielding Rebar Length, Lb.

Consider a section of wall adjacent to the centerline as shown in Figure 5.3. For an increasing uniform load the maximum moment occurs at the center and the steel stress will first reach a value of yield at this position. At adjacent mortar joints the steel stress is defined by the shape of the bending moment diagram. Between the mortar joints the steel stress reduces to some lesser value depending on the stress transferred to the masonry unit by bond.

As the load is increased the steel stress at the yielded joint will increase due to strain hardening. By statics the stress at adjacent joints will increase proportionately and yield will be reached at adjacent joints. At the same time the steel stress within the blocks will also increase and yield will extend beyond the joints. Eventually the strain hardening at the center joint will increase the stress sufficiently that the yield will extend completely through the block. At this point it is probable that bond will be completely lost in this block, especially when the situation is occurring under cyclic loading conditions.

If the value of the bond stress, u, and the steel strain hardening ratio, SHR, are known the points at which yielding will spread may be computed. Figure 5.3 has been computed for values of u = 300 psi and SHR = 1.0%. The successive lines drawn are for strain ratios ($\varepsilon u/\varepsilon y$) in the steel of 0, 10 and 20 times yield respectively. It can be seen that at a ratio of 10, yielding has spread to three adjacent blocks but the steel stress within the blocks remains below yield. At a ratio of 20, yield has been exceeded throughout the 2 blocks adjacent to the

centerline, and at this point bond loss could be assumed for this distance. Therefore the effective yielding rebar length is 16" each side of centerline, for a total of 32".

The value used in the San Onofre, Unit 1 wall evaluation was 9" each side of centerline, for a total of 18". The values computed above show that this situation would occur under relatively modest strain ratios between 10 and 20, or less than this for lower bond stress and/or higher strain hardening. In fact the bond stress would likely be considerably lower due to the effects of cyclic loads.

Thus it is concluded that the value of Lb used is conservative and less than the probable value from theoretical considerations. In the parametric studies in following sections it is shown that the use of this lower value produces conservative results.

5.1.2 Cracked Joint Width, Ljt.

In the parametric studies reported in the following sections it is demonstrated that the joint width Ljt is of minor importance in the final model. It was replaced by the use of 1.5 Icr in the non-yielding portions of the model and thus this section will show that the effective stiffness of 1.5 Icr is a reasonable value.

The results of tests reported in Volume 2 did show an effective stiffness of 1.5 Icr up to yield level. The concrete code ACI-318 provides a method for computing the effective moment of inertia for deflection calculations, based on the gross and transformed moments of inertia and the ratio of maximum moment to cracking moment. This formula is based on very extensive reinforced concrete test programs and is used in this section because of the similarity in the elastic cracked stiffness of reinforced grouted masonry and reinforced concrete.

In Figure 5.4 the deflections under loads up to yield level are computed for the Turbine Building Group I walls. Deflections are based on values of gross moment of inertia, cracked moment of inertia and 1.5 times the cracked moment of inertia for the linear curves. The third order curves formed by the ACI equation have been computed based on 3 values of the ultimate tension stress for the mortar: (1) 40 psi, (2) 1.33 times this value and (3) 1.67 times this value. It is seen that

the deflection at yield predicted by using 1.5 Icr is in quite good agreement with the deflection predicted by these values. Therefore it is demonstrated that the effective stiffness used in the model is reasonable compared with the stiffness obtained by alternative procedures.

5.2 Parameter Studies

The theoretical considerations presented in Section 5.1 indicate that the values used for Lb and Ljt are not arbitrary but are based on engineering principles. Their specific values do have a degree of uncertainty and consequently a series of parameter studies was performed to examine the impact on the response of a masonry wall of variations in the values of both Ljt and Lb. These studies and the results obtained are described in the following sections.

For all studies a 20'-8" wall from the Turbine Building without any added mass was selected. This wall is typical of wall numbers TB-1, TB-5, TB-6 and TB-7 and had the greatest span of all walls included in the evaluation. It also had relatively light vertical reinforcing compared with the Ventilation Building walls. For these reasons the steel strains and the difference between the gross and cracked stiffness were each at a maximum. Therefore it was considered that the greatest effects of variations in Ljt and Lb would be determined by studying this wall.

5.2.1 Effect of Varying Ljt.

The value of Ljt adopted for the original wall evaluation was 2 inches. To study the effect of this parameter the wall was also analyzed with values of Ljt = 0.5", 1.0" and 3". As discussed previously it was expected that the importance of this parameter would be minimized due to the adoption of an effective stiffness of 1.5 times the transformed stiffness for the non-yielding portion of the wall. Ljt was used only in the yielding portion of the wall. Note that for these parametric studies the coordinates of the model were adjusted so that the length of yielding rebar, Lb, remained constant at 18 inches.

The results are summarized in Figure 5.5 and the first part of Table 5.1 in terms of the maximum central deflections and the steel strain ratio or local ductility demand. In general the length of Ljt had little

effect on the values of these response parameters, especially for joint widths from 0.5" to 2". The maximum variation from the values for the "benchmark" 2 inch joint were +3% and -4% in central deflections and +4% and -5% in the steel strain ratios. These differences are not considered significant.

5.2.2 Effect of Varying Lb.

The method of modelling the yielding rebar was studied by varying the length of the single yielding rebar. The element modelling the yielding rebar was modified so as to have lengths of 2", 10", 22" and 30", compared with 18" used in the San Onofre, Unit 1 wall evaluation.

The results are shown in Figure 5.6 and are tabulated in the lower part of Table 5.1. Note that the "benchmark" analysis remains that which used the 2" joint width.

For variable lengths of a single rebar the deflection results "peaked" at a length of 22", where central deflections were 7% greater than for the 18" length. Rebar lengths less than 18" provided smaller deflections and a length of 30" caused slightly greater deflections although less than for 22". The steel strain ratio was inversely proportional to the rebar length as would be expected since the yielding became more concentrated for the smaller rebar lengths. However as discussed in Section 5.1 if $\varepsilon_u/\varepsilon_y$ is greater than 20 yielding would occur over a greater length than that used in the analysis. Consequently the strain ratio results for the 2" and 10" yield lengths indicate that these are not realistic since yielding would occur over a greater length. This was confirmed by the analysis of the SEAOSC tests reported in Section 3.5 which suggested a hinge length of 57".

5.3 Summary

The original parameter studies used to develop the methodology had shown that the effective stiffness of the wall in the non-yielding portion could be modelled using an effective moment of inertia rather than using elements representing all cracked joints. It was therefore expected that the importance of the parameter Ljt would be minimized. This was demonstrated by a series

of parametric studies where variations in Ljt from 0.5" to 3" caused less than 5% variation in response. Deflections computed using the effective moment of inertia from the ACI code confirmed that the effective stiffness used for the non-yielding wall was reasonable.

Theoretical considerations showed that yield would spread out from the point of maximum moment through adjacent masonry units at relatively low steel strain ratios. The value of 18 inches selected for the wall analysis was not arbitrary but was based on engineering judgement. Conservatism was used in evaluating the value of Lb from theoretical considerations and a series of parametric studies were performed to validate the conservatism. The series showed that as the length of yielding rebar decreased deflections tended to decrease and steel strain ratios to increase. For short lengths of yielding rebar the steel strain ratios indicated by the analysis were of such magnitude that bond loss would be certain to occur and therefore the actual yield length would undoubtedly increase inferring that a short rebar yield length is not realistic.

PARAMETER VARIED	VALUE OF VARIABLE	DISPLACEMENT (ins)		STEEL STRAIN RATIO
		MAXIMUM	MINIMUM	
Joint Width Ljt	0.5"	9.56	-9.70	20.5
	1.0"	9.39	-9.67	20.2
	2.0" (1)	9.28	-9.36	19.7
	3.0"	8.88	-9.14	18.7
Rebar Length Lb	2"	7.85	-7.63	124.0
	10"	9.16	-9.18	34.2
	22"	9.97	-10.04	19.1
	30"	9.71	-9.85	13.8

NOTES:

(1) Ljt = 2.0" was used for the evaluation of the San Onofre, Unit 1 walls (Benchmark).

TABLE 5.1 : EFFECT OF VARIABLES IN Ljt and Lb

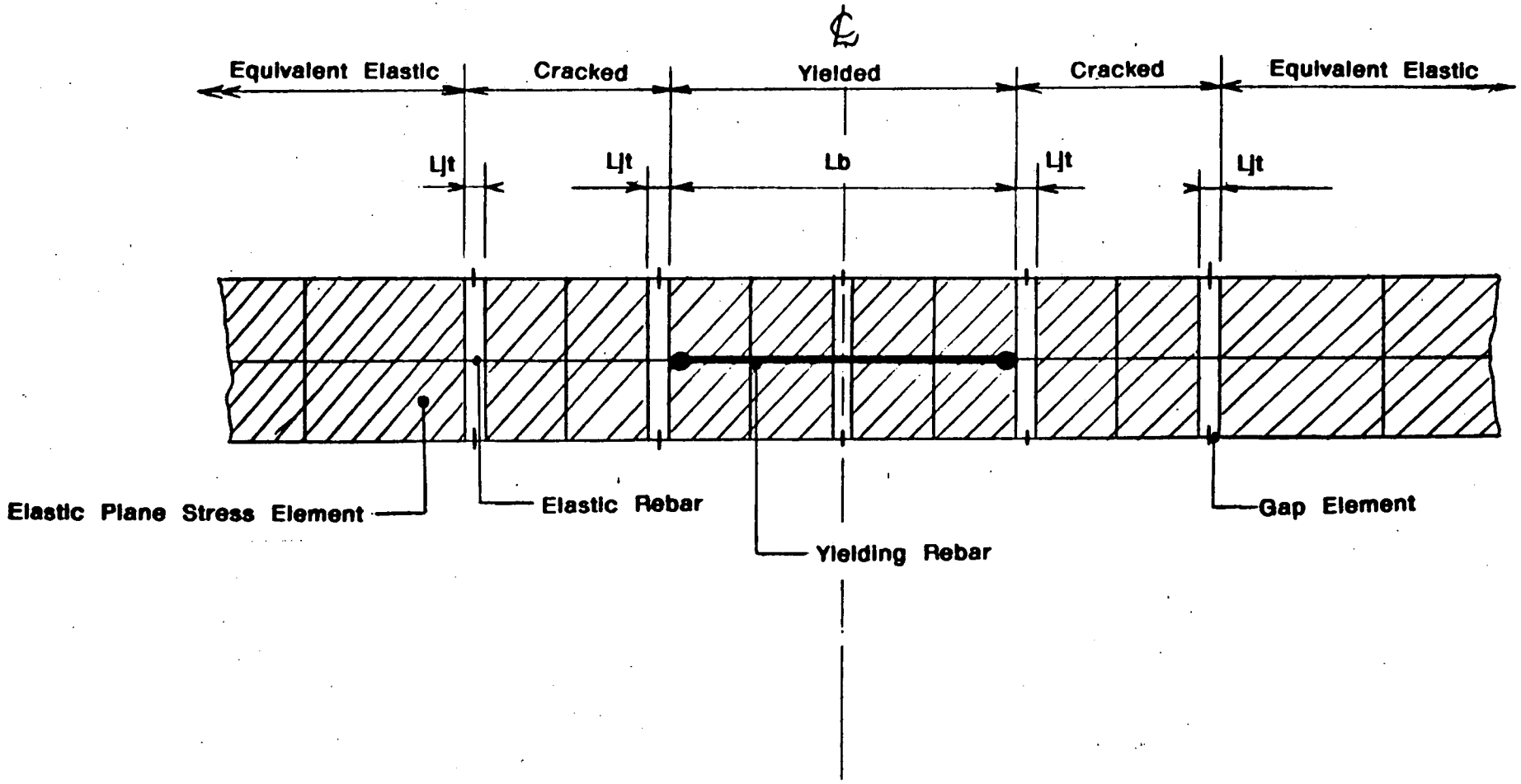

FIGURE 5.1 : INCORPORATION OF Ljt AND Lb IN WALL MODEL

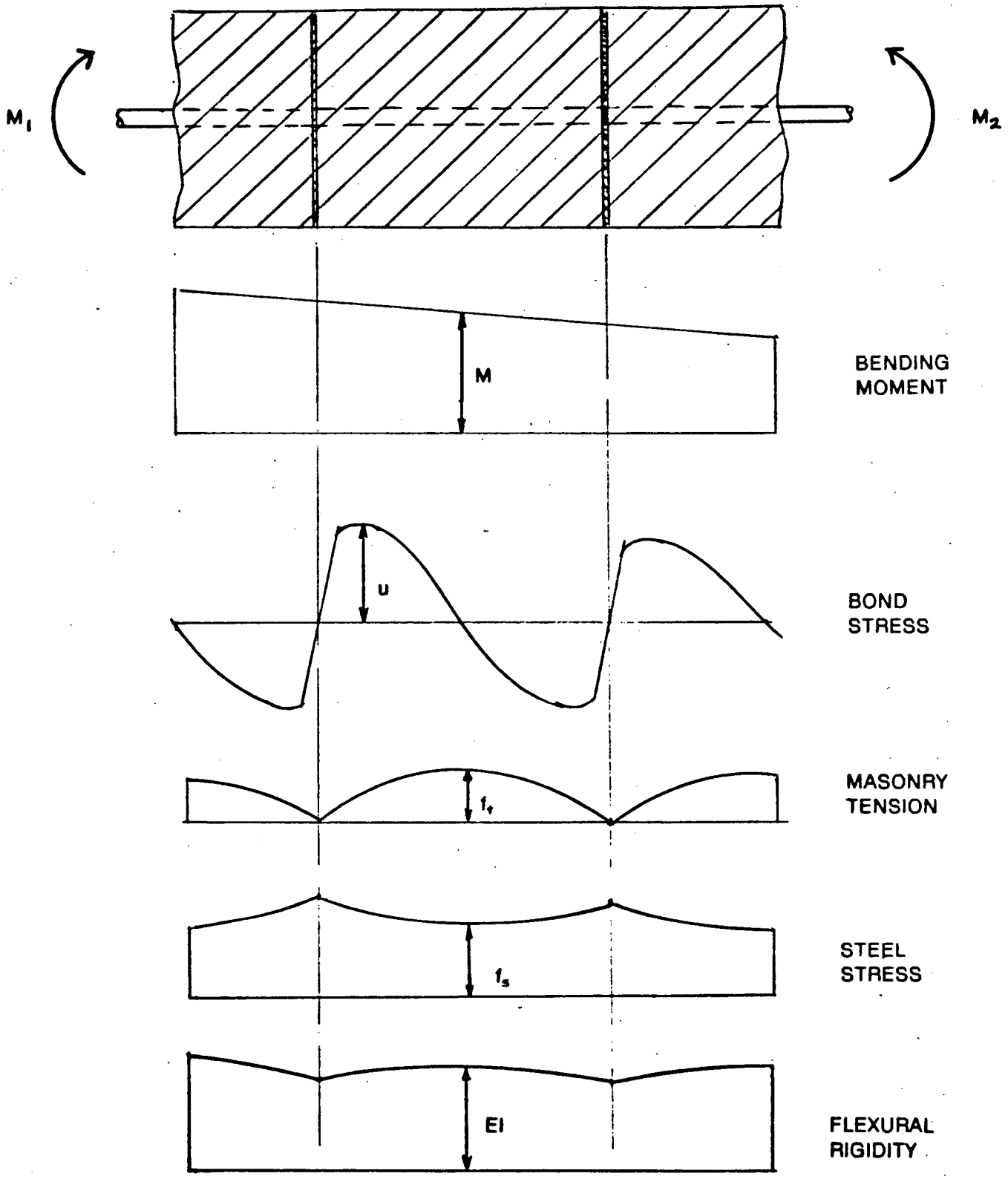

FIGURE 5.2 : EFFECT OF CRACKING

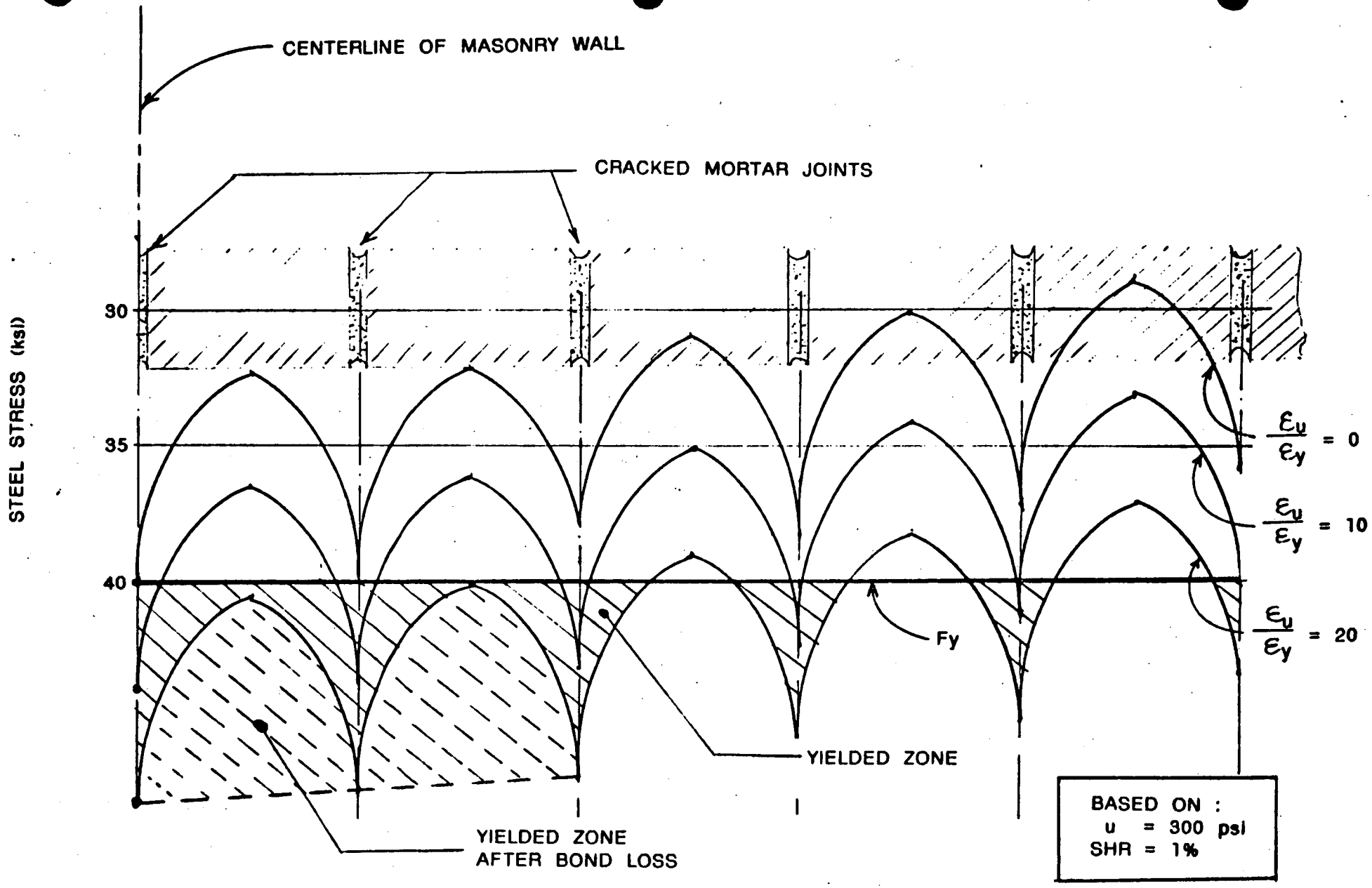

FIGURE 5.3 : INCREASE IN STEEL STRESS AFTER YIELD

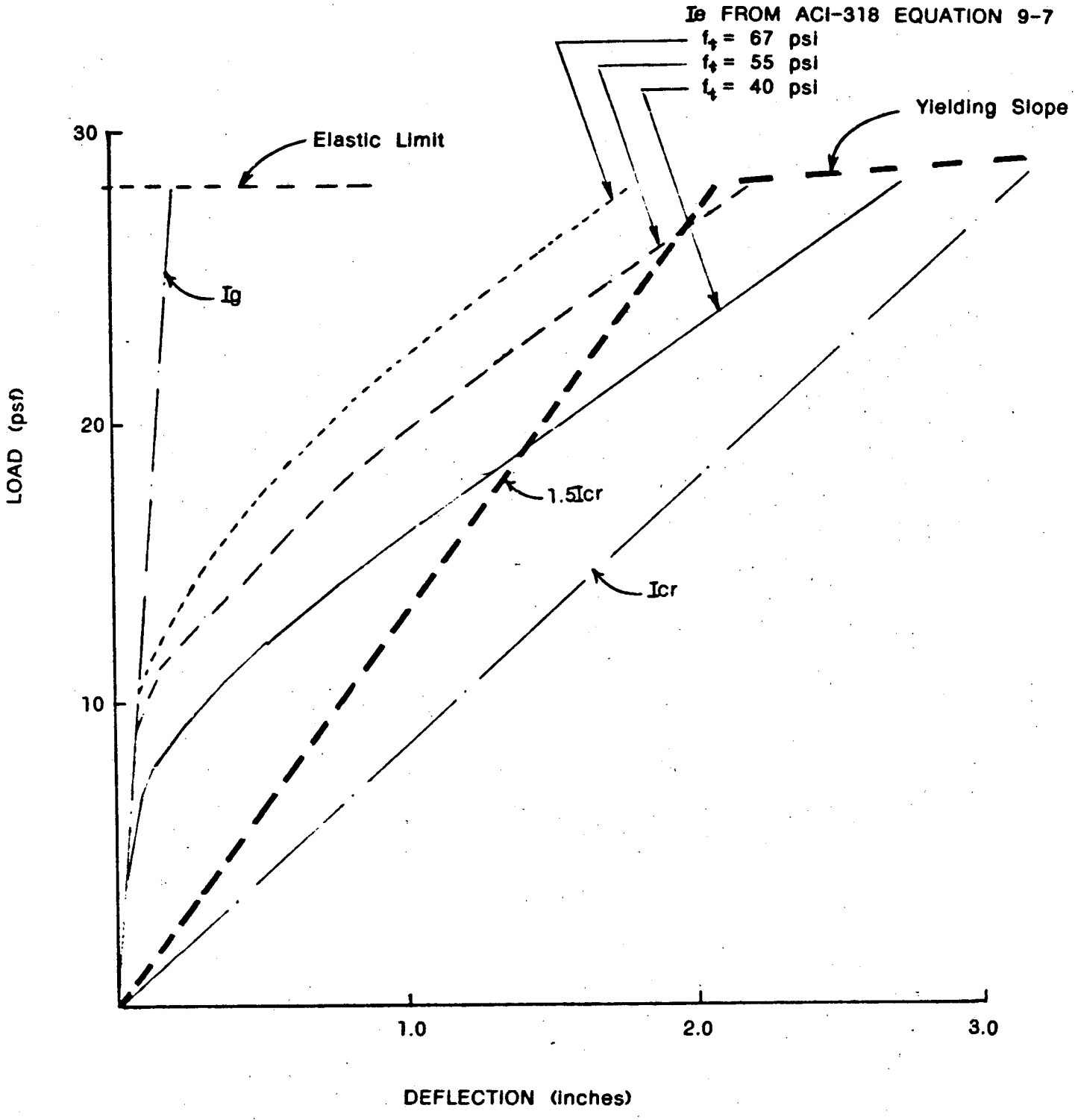

FIGURE 5.4 : DEFLECTIONS UP TO YIELD

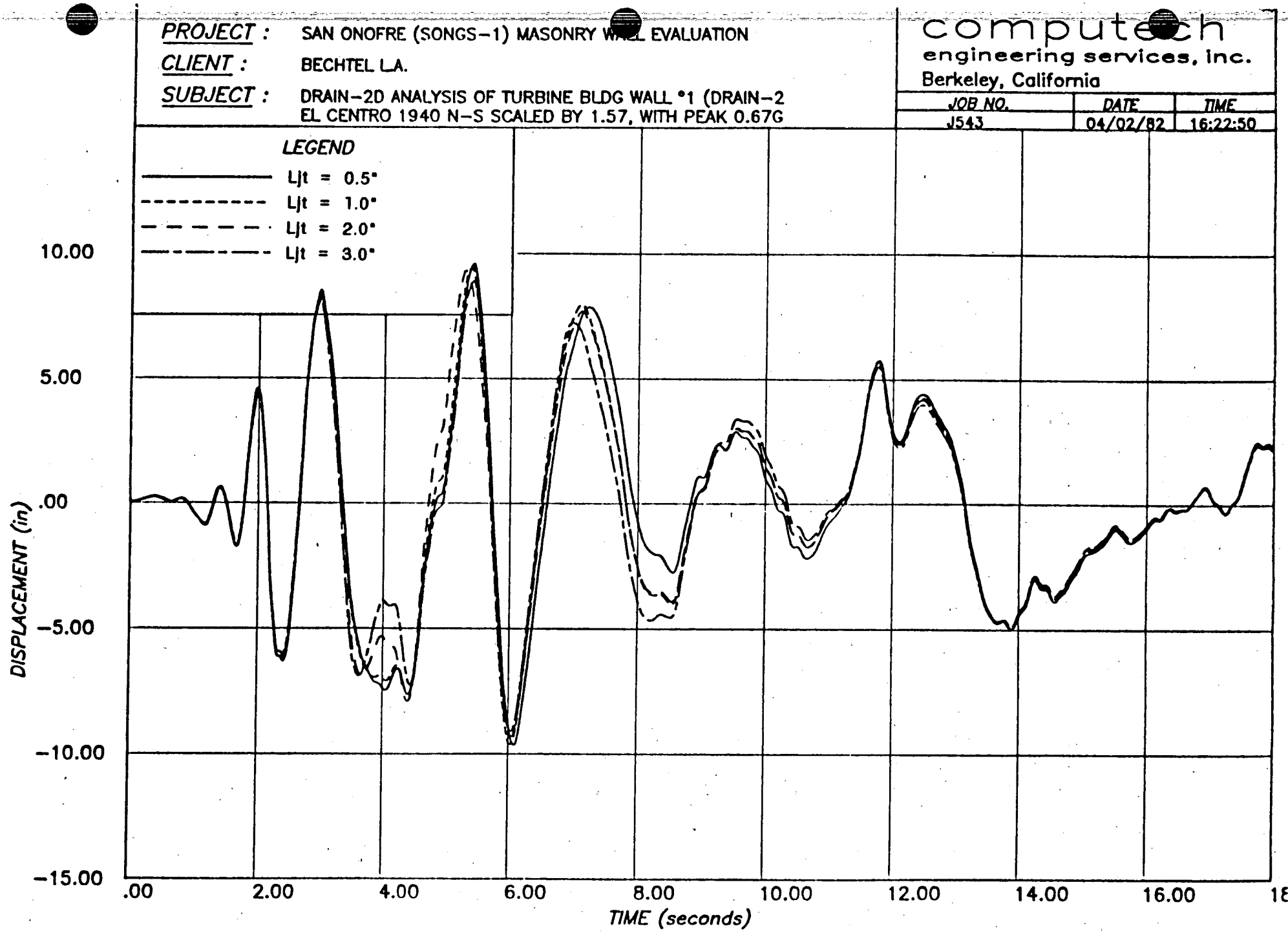

FIGURE 5.5 : EFFECT OF VARIATION IN Ljt

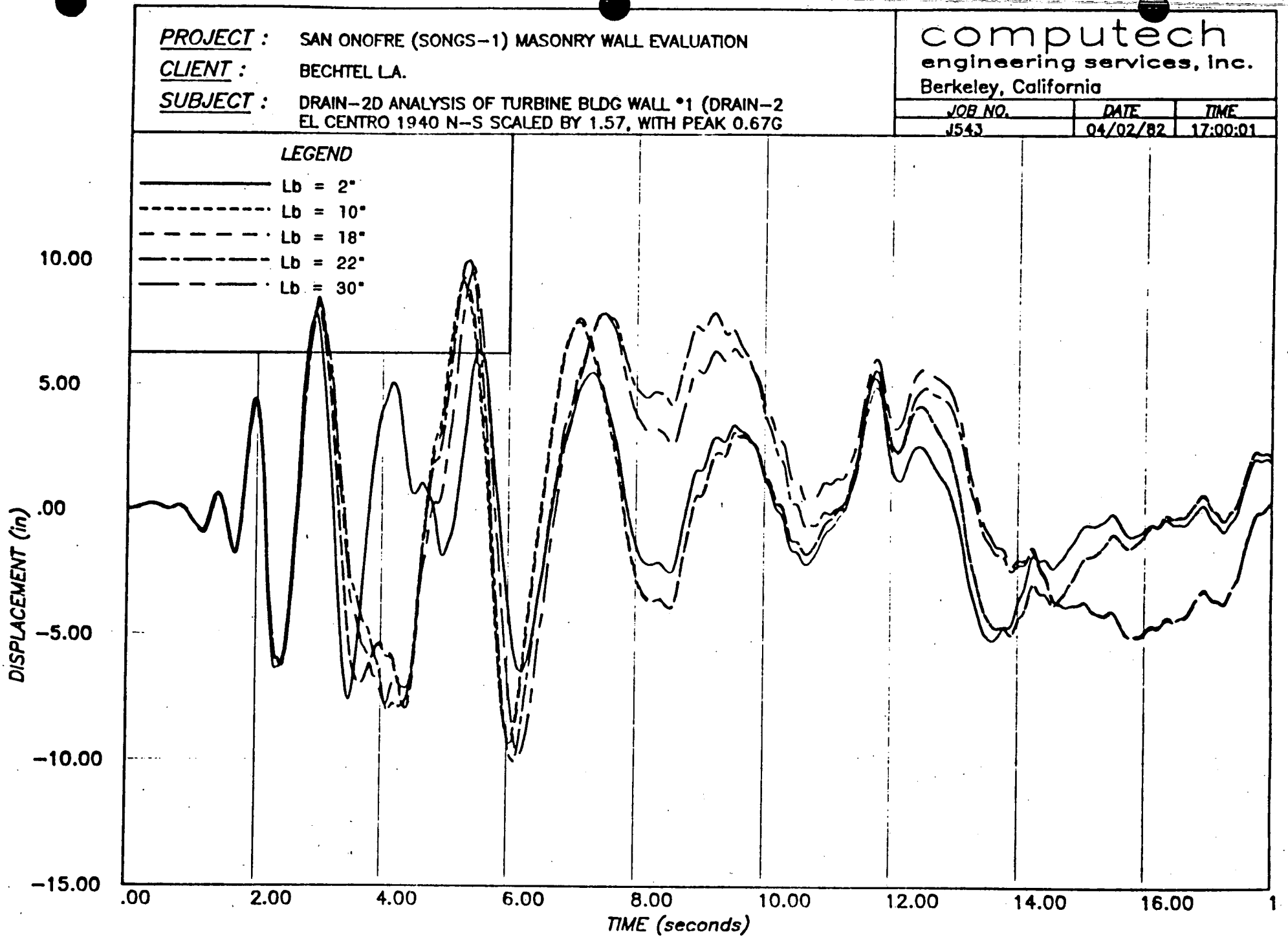

FIGURE 5.6 : EFFECT OF VARIATION IN Lb

6 ITEM 4(d) DISPLACEMENT DUCTILITY

QUESTION:

> "The permissible ductility is only mentioned with respect to quantification of maximum permissible strain in reinforcing steel. However, quantifications of the ductility in terms of force/deflection, moment/curvature (analogous to that given in Appendix C of ACI-349) need to be further examined and their significance discussed."

RESPONSE:

Appendix C of the ACI 349-80 code provides limits of ducilities defined both as displacement and rotational deformation ratios. It also allows that "applicable theoretical or experimental evidence may be used to justify requirements less conservative than those of this appendix." (C.1.4). It is felt that the methodology and criteria developed for the San Onofre, Unit 1 masonry wall evaluation would thus be included under this clause and therefore be presented as an alternative to the appendix provisions.

However, the limitations applied by this code as they apply to the San Onofre, Unit 1 masonry walls have been computed and compared with the maximum values obtained from the time history analyses. In the following section the method used to develop the numerical ductility limits is described. The computation of the equivalent values from the time history results is then discussed. A table comparing the allowable and the maximum values is presented.

6.1 Permissible Ductility Ratios

ACI 349 defines the ductility ratio as the ratio of the maximum acceptable displacement to the displacement at the effective yield point of the structural element. This ductility ratio is limited to a maximum value of:

$$\mu_D \leq \frac{0.05}{(\rho - \rho')} \leq 10$$

This limit may be computed directly from the reinforcing and block dimensions

for each type of wall at San Onofre, Unit 1.

Clause C.3.4 further limits the rotational capacity to 0.0065(d/c), not greater than 0.07 radians. From the commentary this is seen to be the product of the ultimate curvature and the plastic hinge length. The limit on the ultimate curvature is given by

$$\psi u = \varepsilon u / c$$

where c is the distance to the extreme compression fiber and where εu is the ultimate strain obtained from the expression below:

$$\varepsilon u = 0.003 + 0.5/z$$

z is the span distance in inches from the point of maximum moment to zero moment. For simply supported walls z is one half the span length and so for the spans at San Onofre, Unit 1 this equation gives ultimate strains ranging from 0.007 for the highest walls to 0.012 for the low walls in the Reactor Auxiliary Building.

For convenience for comparison with analytical results this can be expressed as a limitation on the maximum curvature ductility, i.e. ultimate curvature divided by the curvature at first yield, where yield curvature is obtained as

$$\psi y = M / EI$$

M is the moment at yield and E and I are the modulus of elasticity and moment of inertia respectively.

For each wall both the displacement and the curvature ductility limits have been computed and compared with the maximum values from the analysis, derived as described in the following section.

6.2 Maximum Values from Analysis

The maximum displacement ductility for each analysis has been obtained directly by dividing the maximum or ultimate deflection by the deflection at the time of first yield at the center of the wall.

The curvature ductility ratio has been obtained by dividing the maximum curvature occurring in the analysis by the yield curvature. The yield curvature has been computed as M / EI as described in the previous section. The maximum curvature has been calculated by dividing the maximum plastic rotation by the plastic hinge length, defined here as the length of yielding rebar. The plastic rotation is obtained by geometry from the maximum plastic deflection and the length of the wall, conservatively assuming a concentrated hinge.

6.3 Comparison of Maximum vs Allowable Ductility

Table 6.1 provides a comparison of the maximum permissible ductilies with the maxima obtained from the analysis for each earthquake record using the most heavily loaded portion of each wall. Both displacement and curvature ductilies are tabulated. Also listed are the maximum permissible values from ACI-349 Appendix C.

For all walls the displacement ductility is less than one half of the allowable values from ACI-349 for all earthquakes. The curvature ducility was less than the allowable values from ACI-349 except for two walls. In two of the Turbine Building walls, TB-9 and TB-10, the maximum curvature ductility of 17.4 under the scaled El Centro earthquake record exceeds the maximum allowable value of 13.9 by about 25%. However the steel strain ratio in all walls was less than the limit of 45 set in the criteria in Volume 1 of the report. The other 2 earthquake records for the same walls produce curvature ductility values approximately 65% of the allowable value.

The relationship between the displacement ductility, the curvature ductility and the steel ductility (steel strain ratio) is illustrated in Table 6.2. In this table the maximum value from the three earthquake records for each ductility is tabulated. Numerically the steel strain ratio is the largest value for the Turbine Building walls and the curvature ductility is higher for the other two building. Displacement ductilities are several times smaller than either of the other two ductilities.

BUILDING	WALL I.D.	PERMISSIBLE		MAXIMUM FROM ANALYSES					
				EL CENTRO		TAFT		OLYMPIA	
		μ_d	μ_ϕ	μ_d	μ_ϕ	μ_d	μ_ϕ	μ_d	μ_ϕ
TURBINE	TB-1a	10	13.9	3.7	13.6	1.5	3.4	2.7	7.6
	TB-1b	10	17.9	2.9	9.6	2.1	5.3	3.3	8.4
	TB-2	10	17.9	1.9	4.8	2.0	5.2	3.4	9.7
	TB-3	10	17.9	1.9	4.8	2.0	5.2	3.4	9.7
	TB-4	10	17.9	1.9	4.8	2.0	5.2	3.4	9.7
	TB-5	10	13.9	3.7	13.6	1.5	3.4	2.7	7.6
	TB-6	10	13.9	3.7	13.6	1.5	3.4	2.7	7.6
	TB-7a	10	13.9	3.7	13.6	1.5	3.4	2.7	7.6
	TB-7b	10	17.9	1.9	4.8	2.0	5.2	3.4	9.7
	TB-8	10	17.9	2.9	9.6	2.1	5.3	3.3	8.4
	TB-9	10	13.9	4.6	17.4	1.7	5.2	2.6	8.9
	TB-10	10	13.9	4.6	17.4	1.7	5.2	2.6	8.9
	TB-11	10	13.9	3.7	13.6	1.5	3.4	2.7	7.6
	TB-12	10	13.2	3.3	10.4	1.1	1.3	2.4	6.3
VENTILATION	VB-1	10	5.7	1.8	5.6	E	E	1.1	2.4
	VB-2	10	5.7	1.8	5.6	E	E	1.1	2.4
	VB-3	10	5.7	1.8	5.6	E	E	1.1	2.4
	VB-4	10	5.7	1.8	5.6	E	E	1.1	2.4
REACTOR AUXILIARY	SB-1	10	13.2	1.9	4.5	1.5	3.1	1.8	4.2
	SB-2	10	13.2	1.9	4.5	1.5	3.1	1.8	4.2
	SB-3	10	19.8	E	E	E	E	E	E
	SB-4	10	13.2	1.9	4.5	1.5	3.1	1.8	4.2
	SB-5	10	19.8	E	E	E	E	E	E
	SB-6	10	19.8	E	E	E	E	E	E
	SB-7	10	13.2	1.9	4.5	1.5	3.1	1.8	4.2

NOTES:

1. Displacement ducility is μ_d
2. Curvature ductility is μ_ϕ
3. Turbine Walls TB-1 and TB-7 are of variable height. Sections marked "a" are 21'-4" high and those marked "b" are 14'-8".
4. "E" indicates elastic response as shown in Volume 3.

TABLE 6.1 : MAXIMUM DUCTILITY RATIOS

BUILDING	WALL I.D.	DUCTILITY		
		DISPLACMENT	CURVATURE	STEEL
TURBINE	TB-1a	3.7	13.6	24.6
	TB-1b	3.3	9.6	12.1
	TB-2	3.4	9.7	13.0
	TB-3	3.4	9.7	13.0
	TB-4	3.4	9.7	13.0
	TB-5	3.7	13.6	24.6
	TB-6	3.7	13.6	24.6
	TB-7a	3.7	13.6	24.6
	TB-7b	3.4	9.7	13.0
	TB-8	3.3	9.6	12.1
	TB-9	4.6	17.4	25.5
	TB-10	4.6	17.4	25.5
	TB-11	3.7	13.6	24.6
	TB-12	3.3	10.4	16.8
VENTILATION	VB-1	1.8	5.6	3.65
	VB-2	1.8	5.6	3.65
	VB-3	1.8	5.6	3.65
	VB-4	1.8	5.6	3.65
REACTOR AUXILIARY	SB-1	1.9	4.5	3.78
	SB-2	1.9	4.5	3.78
	SB-3	E	E	E
	SB-4	1.9	4.5	3.78
	SB-5	E	E	E
	SB-6	E	E	
	SB-7	1.9	4.5	3.78

NOTES:

1. Displacement ducility is $\mu_d = \frac{\Delta_u}{\Delta_Y}$
2. Curvature ductility is $\mu_\varphi = \frac{\varphi_u}{\varphi_Y}$
3. Steel Ductility is $\mu_S = \frac{\varepsilon_u}{\varepsilon_Y}$
4. Turbine Walls TB-1 and TB-7 are of variable height. Sections marked "a" are 21'-4" high and those marked "b" are 14'-8".
5. "E" indicates elastic response as shown in Volume 3.

TABLE 6.2 : MAXIMUM DUCTILITY RATIOS

7 ITEM 4(e) AIR BAG TESTS

QUESTION:

> "It is doubtful that the air bag used in test to load walls provides a uniform pressure on the surface of the wall as intended. It is unclear that the wall be analyzed as a cantilever beam, a compressed beam, or as a slab with different edge conditions."

RESPONSE:

The details of the SEAOSC tests were provided solely to illustrate that the integrity of a well anchored and reinforced masonry wall is maintained even when deflections considerably exceed the wall thickness. The results were not used for any purpose beyond this and were not included as part of the model verification.

For this reason it is maintained that the actual pressure distribution on the wall is not of major importance. It is possible that at high deflections the contact will not be uniform along the wall height but nevertheless the demonstration of structural integrity is not altered.

8 ITEM 4(l) COMPUTER PROGRAMS

QUESTION:

> "Details of computer codes are not known. Degree and order of accuracy, error propogation, numerical stability, integration schemes and all pertinent verification data for numerical analysis should be provided for assessment of the computer codes. Are there any numerical damping induced to the solution. How does it compare with the system damping."

RESPONSE:

In the following sub-sections the computer codes used for the evaluation are presented and the accuracy and numerical stability of the solutions are discussed. The results of analyses to demonstrate these facets are given and numerous references are provided.

8.1 Computer Codes

The two computer codes used for all wall analyses were DRAIN-2D and ANSR-II. Both these programs were developed at the University of California, Berkeley and have been in general use for a number of years. The basic references for these programs [8.16, 8.17, 8.18, 8.19] detail the solution strategies and provide verification examples for the programs. In the following sub-sections specific details of these codes are summarized.

8.2 Accuracy of Solution

The accuracy of a time history analysis is assessed by measuring the amplitude and frequency distortion as a function of the sampling rate when a scheme is applied to the solution of an undamped linear oscillator. The errors associated with the time step choice have been shown to grow rapidly as the time step is increased [8.9]. For linear problems utilizing the trapezoidal rule, equilibrium is satisfied at the time step intervals but not within the steps. If equilibrium were satisifed at all times the exact response would be obtained, which is not the case.

However, for non-linear problems equilibrium errors may be present at the beginning of any time step. These errors can occur if the structural stiffness and/or viscous damping matrix change at the end of the preceding time step because of material nonlinearity. Therefore for non-linear problems the accuracy of the solution is directly related to how well dynamic equilibrium is satisfied. In general the accuracy of the solution is inversely related to some norm of the unbalanced force vector. This norm of unbalanced force may be reduced by decreasing the time step (i.e. second order of accuracy [8.10]), by iteration or by use of an event-to-event solution strategy.

DRAIN-2D uses a combination of equilibrium correction and event-to-event strategies. ANSR-II uses iteration and equilibrium corrections. The accuracy of the solution using the latter program has been assessed by repeating the same analysis with a reducing time step. There was very little difference between the larger and smaller time steps (Figure 8.1) and therefore the accuracy of the solution strategy is assured.

Greater accuracy has been shown to be possible by controlling the equilibrium error in the middle of the time step [8.11]. A new version of DRAIN-2D has been released wih this feature to improve accuracy. This enhanced program, DRAIN-2D2 [8.12], uses an automatic time step selection scheme, where the time step size is adjusted based on the maximum norm of the midstep equilibrium unbalanced vector (the "midstep error"). To provide a further check on the accuracy of the results the problem was repeated using DRAIN-2D2 with specifed maximum tolerances of 20k and 40k on the midstep error. This provided virtually the same response as that predicted by the original version of DRAIN-2D, as shown in Figure 8.2

8.3 Numerical Stability

The stability of a solution may be assessed by studying the amplitude growth of the computed solutions to linear and non-linear problems. Whereas the stability of integration operators have been established for linear systems [8.2 to 8.8] additional considerations are required for non-linear systems. In general the stability of a linear system is a numerical problem related to the spectral radius of the integration operators of the different schemes. However, for non-linear analyses the source of instability is more complex and results in amplitude increase and hence in the accumulation of energy errors.

The Newmark methods are unconditionally stable for $\gamma \geq 0.5$ and $\beta \geq 0.25(\gamma + 0.5)^2$, which is the case for the trapezoidal rule.

For non-linear problems assessment of the energy error is a good indication of the stability of the system [8.13, 8.14]. DRAIN-2D2 has therefore been used to calculate the growth of energy and prints the energy values at each step so that stability problems can be identified [8.12]. In addition, the program provides a breakdown of the contribution of each component to the overall energy balance as follows:

1) Elastic Energy : Recoverable energy absorbed by the elements.

2) Plastic Energy : Non-recoverable energy absorbed by the elements.

3) Damping Energy : Energy absorbed by damping effects.

4) Kinetic Energy : Energy stored by the velocity of the concentrated nodal masses.

5) Static Energy : Energy input to the system through work done by static loads

6) Dynamic Energy : Energy input to the system through inertia forces caused by ground accelerations.

7) Energy Error : The difference between the totals of the input and the absorbed energy, i.e. (5+6)-(1+2+3+4).

The examples analyzed using DRAIN-2D2 as described above showed a maximum energy error of 0.3%. This is much less than the precentage which has been found to indicate instability, which is in excess of 10%.

8.4 Numerical Damping

In many structural dynamics problems only low mode response is of interest. Finite element discretization introduces high frequency modes which are physically meaningless and which should not be allowed to participate in the solution. Therefore for only low mode response it is often advantageous for an algorithm to possess some form of numerical damping to dampen

participation of these higher modes. However, most algorithms with numerical damping also introduce extensive damping into the lower modes and thus make the solution inaccurate. Wilson's method, with θ = 1.4, produces 7% damping at dt/T = 10 and thus is too dissipative in the lower modes. To avoid this phenomenon a new family of unconditionally stable integration methods for linear systems has been introduced by Hilber, Hughes and Taylor [8.10, 8.15]. This is called the α-dissipation method, where the parameter a introduces numerical damping which dampen the higher modes only and does not introduce the lower mode damping of the Wilson method. However the method is complicated and does not satisfy equilibrium at the end of the time step.

The Newmark family of methods allows the amount of dissipation to be controlled by a parameter other than the time step and when the quantity γ is taken as 0.5 there is no numerical damping. This is the case for both DRAIN-2D and for ANSR-II. Therefore the only damping present in each of these programs is physical damping introduced through stiffness and/or mass porportional damping. For fixed initial stiffness proportional damping values damping of the spurious higher modes at least comparable to the α-dissipation method is provided. Therefore it is concluded that the trapezoidal scheme with stiffness damping which introduces no numerical damping is superior for the DRAIN-2D and ANSR-II types of application.

8.5 References

[8.1] Newmark, N. M. "A Method of Computing for Structural Dynamics", Journal of Engineering Mechanics Division, A.S.C.E., Vol 85, pp 67-94, 1959.

[8.2] Nickell, R. E. "On the Stability of Approximation Operators in Problems of Structural Dynamics", International Journal of Solids and Structures, Vol. 7, pp. 301-319, 1971.

[8.3] Goudreau, G. L. and Taylor, L. R. "Evaluation of Numerical Integration Methods in Elastodynamics", Computer Methods in Applied Mechanics and Engineering, Vol. 2, No. 1, pp.

69-97, 1973.

[8.4] Bathe, K. J. and Wilson, E. L., "Stability and Accuracy Analysis of Direct Integration Methods", International Journal of Earthquake Engineering and Structural Dynamics, Vol 1, pp. 283-291, 1973.

[8.5] Kreig, R. D., "Unconditional Stability in Numerical Time Integration Methods", Trans. A.S.M.E., Journal of Applied Mechanics, pp. 417-421, June 1973.

[8.6] Johnson, D. E., "A Proof of the Stability of the Houbolt Method", A.I.A.A. Journal, Vol. 4, pp 1450-1451, 1966.

[8.7] Destefano, G. P., "Causes of Instabilities in Numerical Integration Techniques", International Journal of Computational Mathematics, Vol. 2, pp. 123-142, 1968.

[8.8] Bathe, K. J., and Wilson, E. L., "Numerical Methods in Finite Element Analysis", Prentice-Hall, Englewood Cliffs, New Jersey, 1976.

[8.9] Wu, R.W.H. and Witmer, E.A. "Nonlinear Transient Response of Structures by the Spatial Finite Element Method", A.I.A.A. Journal, Vol 11, No. 8, pp. 1110-1117, 1973.

[8.10] Hilber, H.M. "Analysis and Design of Numerical Integration Methods in Structural Dynamics", Ph.D Dissertation, Department of Civil Engineering, University of California, Berkeley.

[8.11] Hibbitt, H.D. and Karlsson, B.I. "Analysis of Pipe Whip", A.S.M.E. publication for presentation at Pressure Vessels and Piping Conference, San Francisco, California, June 25-29, 1979.

[8.12] Golafshani, A., and Powell, G.H., "DRAIN-2D2

A Program for Inelastic Seismic Response of Structures", University of California, Berkeley, Report No. EERC/82-, 1982. (To Be Published)

[8.13] Hughes, T.J.R., Caughey, T.K., and Liu, W.K., "Finite Element Methods for Nonlinear Elastodynamics which Conserve Energy", Journal of Applied Mechanics, Vol. 45, pp. 366-369, 1978.

[8.14] Ghose, A., "Computational Techniques for Inelastic Dynamic Analysis", Ph. D Thesis, Department of Civil Engineering, University of California, Berkeley, 1976.

[8.15] Hilber, H.M., Hughes, T.J.R., and Taylor, R.L., "Improved Numerical Dissipation of Time Integration Algorithms in Structural Dynamics", Earthquake Engineering and Structural Dynamics, Vol. 5, pp. 282-292, 1977.

[8.16] Kanaan, A. and Powell, G.H., "General Purpose Computer Program for Inelastic Dynamic Response of Plane Structures", University of California, Berkeley, Report No. EERC/73-6, 1973.

[8.17] Powell, G.H., "DRAIN-2D User's Guide", University of California, Berkeley, Report No. EERC/73-22, 1973.

[8.18] Mondkar, D.P., and Powell, G.H., "ANSR-I General Purpose Computer Program for Analysis of Non-Linear Structural Response", University of California, Berkeley, Report No. EERC/75-37, 1975.

[8.19] Mondkar, D.P., and Powell, G.H., "ANSR-II Analysis of Nonlinear Structural Response, Users Manual", University of California, Berkeley, Report No. EERC/79-17, 1979.

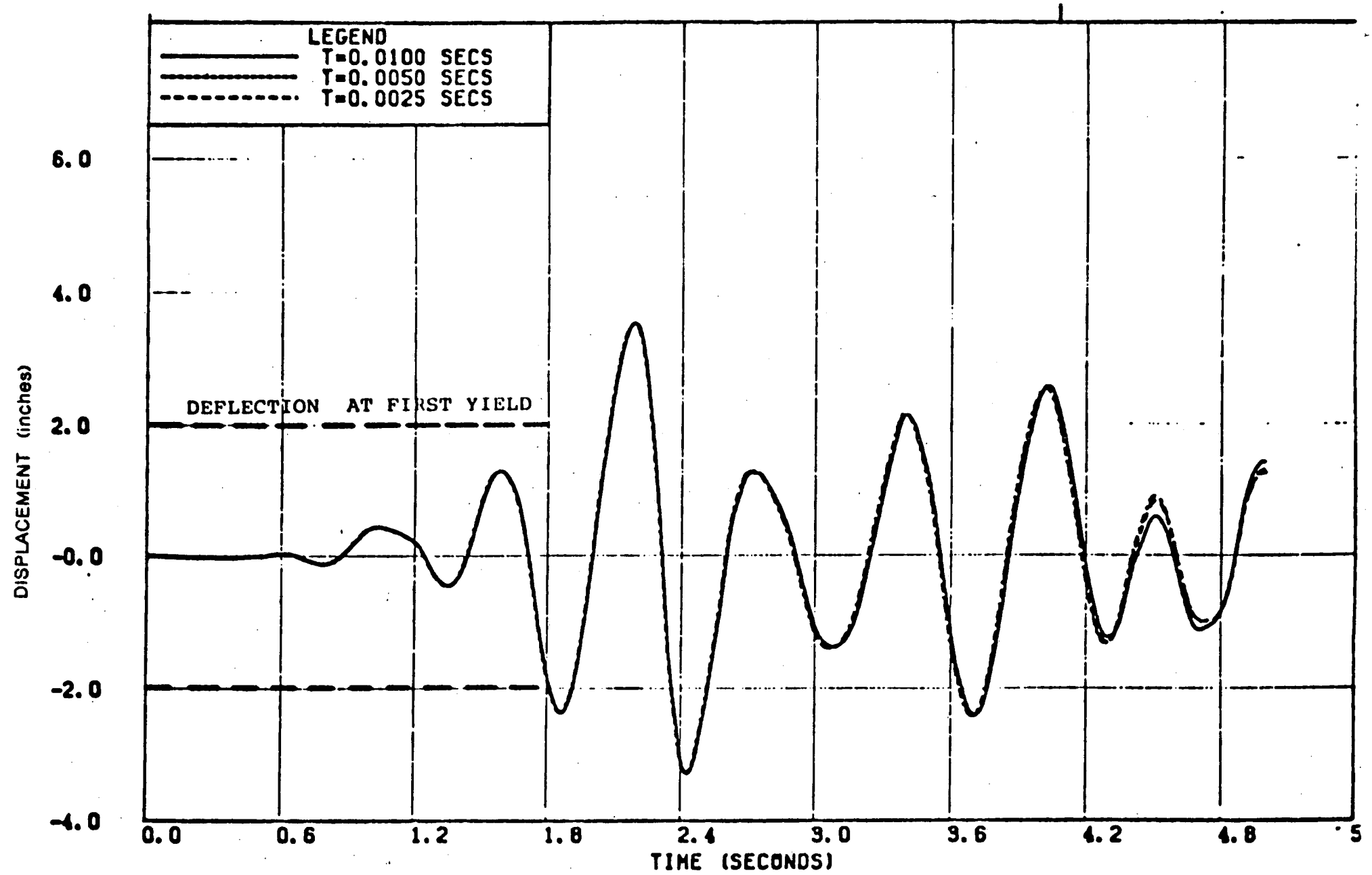

FIGURE 8.1 : EFFECT OF VARIATION IN TIME STEP

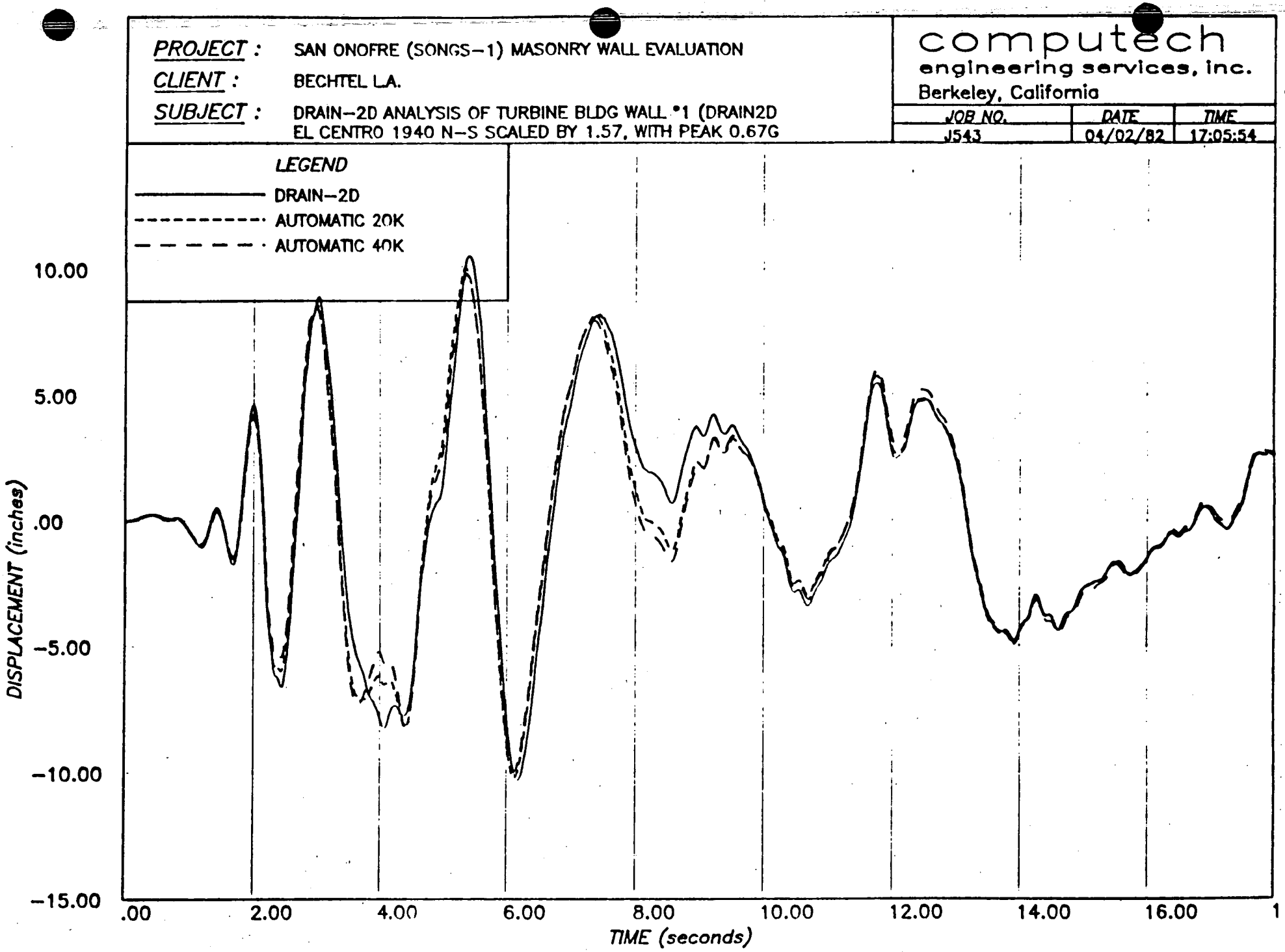

FIGURE 8.2 : EFFECT OF TOLERANCE ON MID-STEP ERROR

9 ITEM 4(g) COMBINED LOADS

QUESTION:

"Assessment of the impact of transverse load on in-plane carrying capacities, and vice versa, is needed."

RESPONSE:

A discussion of the impact of combined loads on the masonry walls is given in the commentary to the criteria in Section 3.3 of Volume 1 of the report. This discussion considers all the possible combinations of the in-plane modes of behavior with the concurrent effects of out-of-plane loadings. Because the major impact of the out-of-plane loads is on the horizontal plane at or about the wall mid-height it is concluded in that commentary that the only additional effect which must be checked for the combined load case is the compression in the face shell due to the in-plane bending moment at the wall mid-height. For walls in double curvature the in-plane moment is zero and thus the additional compression is negligible. For walls in single curvature the compression must be computed.

In the following section the compression stresses due to in-plane loadings are considered for the two types of in-plane loading at San Onofre, Unit 1:

1. Walls required to provide lateral load resistance to the building, e.g. Ventilation Building.

2. Walls with connections such that the only in-plane loads are due to the wall self-weight such as in the Turbine Building.

For the most severely loaded wall in each of these two buildings numerical limits on the simultaneously applied in-plane shear based on the assumed spalling strain are computed.

9.1 Turbine Building Wall TB-9

Wall TB-9 is subjected to the greatest face shell strain, as shown in Table 3.1. The stress and strain distributions under 100% out-of-plane loading are as shown in Figure 9.1.

As simultaneous in-plane loadings are applied the strain will increase parallel to the out-of-plane strain until the spalling limit strain of 0.0040 is reached, as shown in Figure 9.1. Therefore the maximum allowable in-plane loads are such as to cause an increase in strain from 0.00353 to 0.00400. The maximum compression per unit length of face shell may then be computed as the difference between the areas of the two stress distributions.

From the stresses in Figure 9.1 this incremental compression has been computed as 64 lb/inch. As the wall is effectively rigid in-plane and subjected to a uniform acceleration the loading is a uniformly distributed load up the wall height. Therefore a relationship between the acceleration level, a, and the maximum extreme fiber compression, fc, may be derived as shown in Figure 9.3.

For wall TB-9 the height is 20 feet and the weight constant at 61 psf and so the maximum acceleration may be computed as:

$$a = 0.02085\ L$$

where a is the maximum acceleration in g's
L is the wall length in feet.

This gives allowable values from 0.42g for a 20 foot long wall to 0.83g for a 40 foot length. This is the in-plane load applied concurrently with 100% of the out-of-plane loads and so represents 40% of the total in-plane loads, in accordance with the specified load combinations. Thus the effective acceleration limits are 1.04g and 2.08g for the 20 and 40 foot wall lengths respectively. These values are considerably higher than the specified ZPA of 0.67g, and higher than the amplified peak of 0.93g for 7% damping.

One of the Turbine Building walls, TB-5, has a length of only 10'-0". However the strain in this wall due to out-of-plane loads is lower, 0.00295. This allows an incremental compression of 185.8 lb/in, and the expression in Figure 9.3 gives an allowable acceleration of 0.61g under combined loads, i.e. 40% of in-plane loads. Therefore the total allowable in-plane load is that corresponding to 1.53g, again higher than the maximum amplified peak.

9.2 Ventilation Building Wall VB-1

A similar procedure may be followed for the Ventilation Building wall VB-1,

where the stresses and strains due to 100% of out-of-plane loads are as shown in Figure 9.2. These walls are more heavily reinforced than the Turbine Building walls and have considerably smaller maximum deflections. Therefore the strain diagram extends further across the face shell.

When the strain is increased parallel to the limit of 0.00400 the neutral axis falls slightly inside the face shell and so the stress diagram is truncated as shown in Figure 9.2. For these lateral load resisting walls it has been assumed that the full load is applied at the top of the wall and an equation formulated to obtain the limiting in-plane moment at the mid-height in terms of the applied shear force.

This maximum shear is V = 0.829 x L x L, where L is the wall length in inches and V is the limiting in-plane shear in pounds. The Ventilation Building walls are 44 feet and 21 feet long giving maximum shears of 231.1 kips and 52.6 kips. These values represent 40% of the in-plane loads, and therefore the total shear force limits on the walls are 577.8 kips and 131.6 kips respectively. These values are much higher than the limits applied by the purely in-plane modes of behavior and thus flexure at mid-height is not a critical design case.

9.3 Summary

The face shell compressive stresses and strains as derived in Section 3 of this response have been extended to include the effects of concurrent in-plane loading. Numerical examples have been computed for the two most critically loaded wall types.

The in-plane forces in the Turbine Building walls are generated by the self-weight of the walls and they are able to withstand acceleration levels greater than the maximum spectral acceleration before the limiting strain is reached. In the Ventilation Building in-plane forces are generated by the response of the building and the limit occurs at shear levels higher than those permitted by the purely in-plane modes of behavior. Therefore the combined loadings do not have an adverse impact on the wall response.

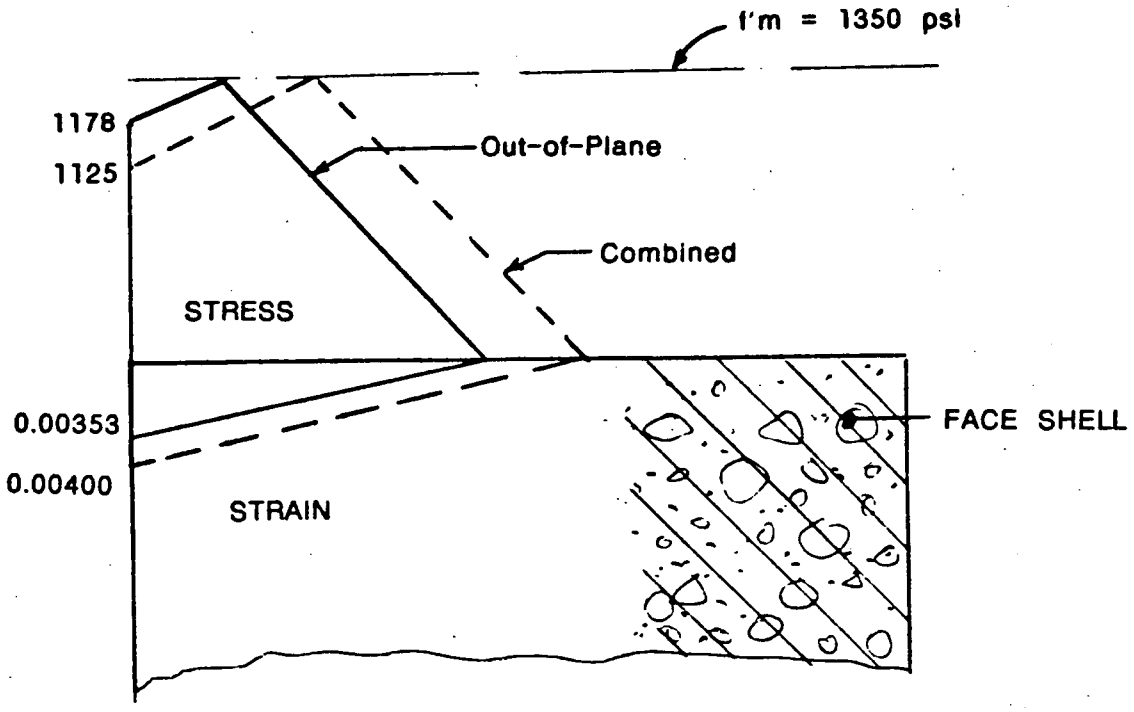

FIGURE 9.1 : COMBINED LOAD ON WALL TB-9

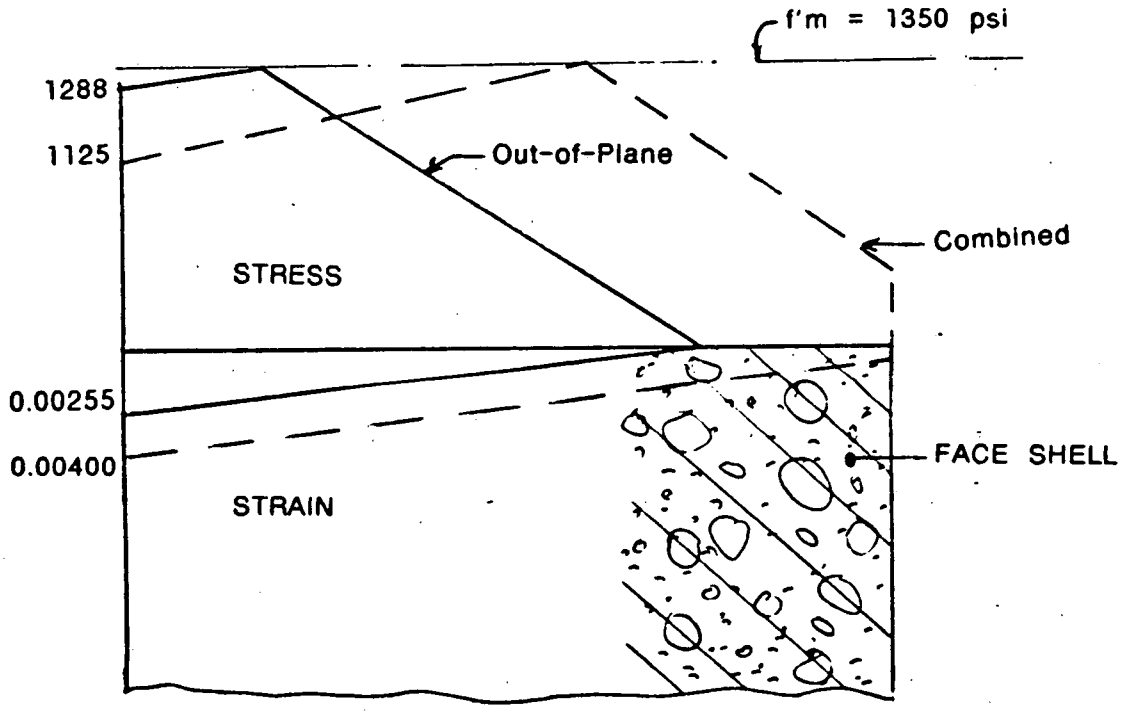

FIGURE 9.2 : COMBINED LOAD ON WALL VB-1

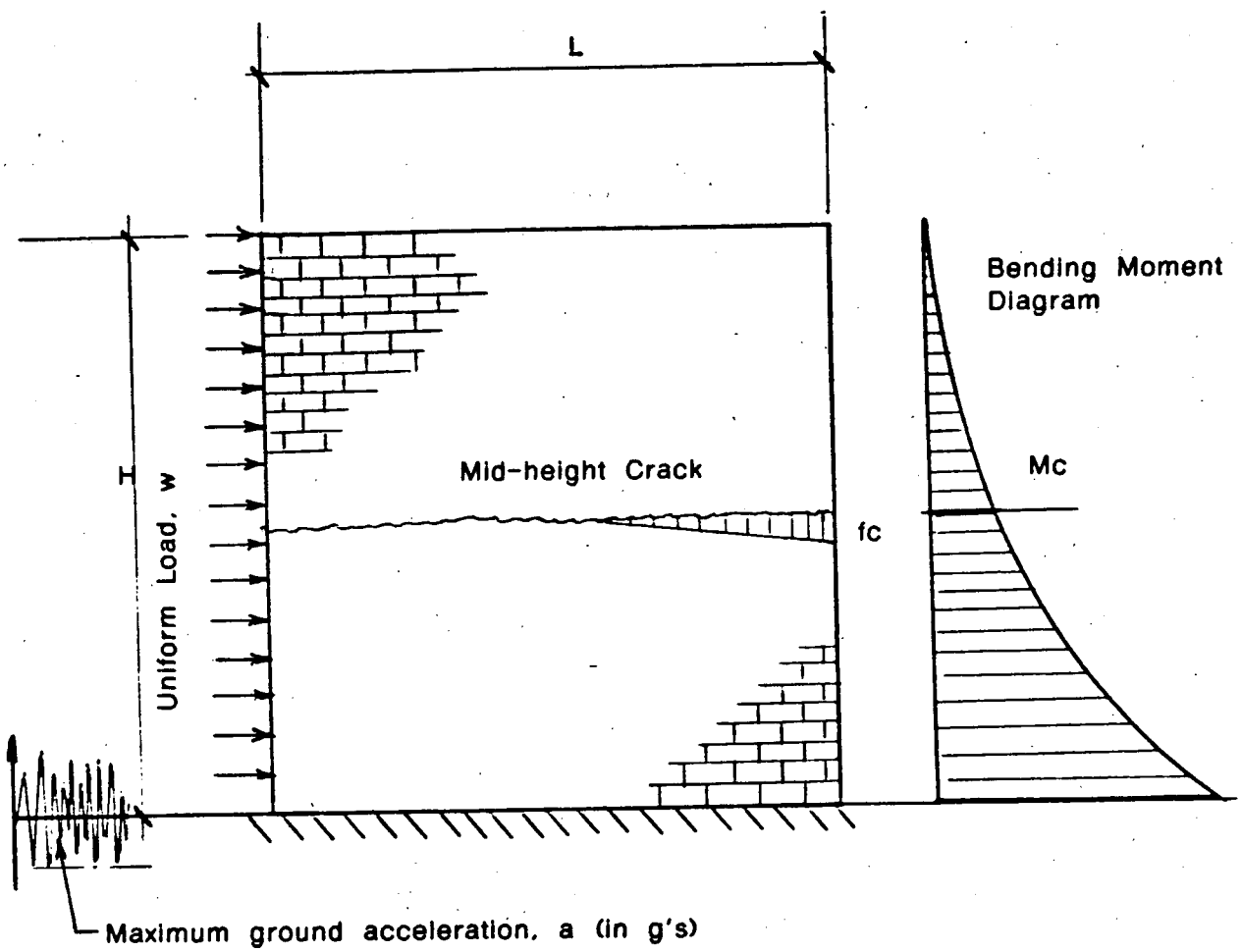

W = Wall weight, psf

w = WLa

Mc = (WLaH**2)/4

fc = M/S (lb/in) where S = L**2/6

fc = (6WLaH**2)/(4L**2)

therefore

a = (2fcL)/(3WH**2)

using

fc = 63.6 lb/inch

W = 61 psf

H = 20 ft

a = 0.02085 L

(L in feet)

FIGURE 9.3 : TURBINE WALL IN-PLANE LOADS

10 ITEM 4(h) WALL ATTACHMENTS

QUESTION:

> "The local and gross effects of attachments on the wall (such as conduit, piping and equipment) were not properly considered in the analysis. The evaluation of the effect of possible local damages and gross motion of the attachment on the overall analysis of the wall is needed."

RESPONSE:

In the following sections this item is addressed in terms of both local effects and overall effects on the wall evaluation based on the support conditions, the strength of the connections and the weight of the equipment.

10.1 Local Effects of Attachments

The type of attachment used to fasten equipment, piping conduit etc. to the masonry walls varies throughout the plant. However a typical type of attachment is very commonly used and the local effects of this are considered below. This evaluation is restricted to the local effects of the tension on the attachments caused by horizontal earthquake accelerations applied at the level of the connection. Connections which do not fall into this category are evaluated on an individual basis in the appropriate portions of the SEP evaluation.

In a number of connections equipment is fastened to the wall by 2-0.5" bolts passing through ungrouted cells and anchored by bearing plates on the opposite wall face. This type of attachment has the potential for two types of local failure mode under direct tension caused by horizontal earthquake motions.

The first potential failure mode is local failure of the masonry face shell beneath the bearing plate. This is a "punching shear" type of failure and the capacity of the face shell has been determined using procedures similar to that used for concrete, i.e. an allowable shear of $4\sqrt{f'm}$ around the perimeter of the loaded area, in this case the bearing plate. For an f'm of 1350 psi and a 3" by 5" bearing plate (typical at San Onofre, Unit 1)

the allowable punching shear is 147 psi giving a connection capacity of 3860 lbs in tension per bolt.

For local block pullout to occur the allowable shear stress in the mortar joint surrounding the block must be exceeded. The allowable shear for this type of loading has been taken as the UBC value for flexural shear, 40.4 psi for an f'm of 1350 psi. The area of the shear plane is 60 square inches for a single block, i.e. two horizontal joints plus two header joints times twice the face shell thickness. This produces an allowable tension on the connection of 2420 lbs.

The minimum of these two values, 2420 lbs, therefore governs the tensile strength of the connection. This is higher than the UBC factored limit of 1650 lbs for 2 bolts. An upper bound on the loads on these attachments would be a 16'-0" run of 24" heavily loaded cable tray, giving a total weight of 852 lbs. Such a length with only one support is likely to exceed that which would actually occur in the plant.

The capacity of the connection is such that it could accomodate a maximum acceleration of 2420/852, or 2.84g. This is higher than the acceleration levels likely to be experienced by wall mounted equipment at San Onofre, Unit 1.

10.2 Overall Effects of Attachments.

The effects of added equipment weights were included for all wall analyses. Because the equipment is rigid their effect could be modelled by adding masses at the appropriate model nodal points. For each evaluation the most severe case of added mass occurring on a particular wall configuration was used on the assumption that the added loads would more than outweigh the effect on the frequency of a more lightly loaded wall.

To validate this assumption each of the three groups of walls in the Turbine Building was re-analyzed with a much lower precentage of added mass. For the re-analysis the total added mass was taken as 25% of the maximum value. This would be typical for the majority of the walls, which have only minor conduit etc mounted on them. For each of the three groups the maximum displacements were reduced. The values for the analyses using the lower added mass were 82%, 93% and 87% of the original analysis values for groups I, II and III respectively.

From these results it is considered that the method used in the evaluation to take account of equipment, attachments etc. is reasonable and conservative.

10.3 Summary

A common form of connection used for the attachment of piping, conduit, cable trays etc. to the walls has a capacity considerably in excess of the maximum acceleration to which the equipment is likely to be subjected. Therefore local failure of the wall at the point of attachment will not occur under horizontal earthquake loads. The analyses performed for the wall evaluations used upper bound values for added weights and the more typically loaded walls had displacements lower by between 8% and 18%.

11 CONCLUSIONS

This report has presented a brief overview of the analysis methodology for the San Onofre, Unit 1 reinforced concrete masonry wall evaluation and addressed each of the technical questions raised by the NRC with respect to this evaluation. Following is a brief summary of the conclusions reached on each of these items.

a. **ITEM 4(a)** Masonry Face Shell Stresses: The stress strain distribution was computed in the face shell for each of the walls evaluated. The maximum strains were less than an ultimate value of 0.004 derived from test data on plain concrete and much less than the limits specified in Appendix C of ACI-349. Results from a series of SEAOSC tests were also processed and showed strain levels at least as high as at San Onofre, Unit 1 with no evidence of spalling.

b. **ITEM 4(b)** Damping: Justification of the specified material damping of 7% was presented. Details of the means of implementing this damping into the nonlinear model were provided and plots of energy balance used to demonstrate that the total effective dissipation due to viscous damping was less than for an equivalent elastic system.

c. **ITEM 4(c)** Rebar Length and Joint Width: Theoretical considerations were used to confirm the validity of the overall model stiffness. Considerations of bond suggested that a conservative approach had been adopted for the length of yielding rebar. A series of parameter studies showed that the effect of the joint width in the final model was minimal and that any increase in yield length would reduce the maximum strains.

d. **ITEM 4(d)** Displacement Ductility : Values of the displacement and curvature ductilities were computed in terms of the formulation in Appendix C of ACI-349. All displacement ductility values for the San Onofre, Unit 1 walls were less than the code limits as were the curvature ductilities for all but two walls.

e. **ITEM 4(e)** Air Bag Tests : A discussion of the significance of the tests performed by SEAOSC was presented.

f. **ITEM 4(f)** Computer Programs: Details of the computer codes used and their accuracy and numerical stability were listed. A number of parametric studies were used to demonstrate the stability of the solutions.

g. **ITEM 4(g)** Combined Loads : Maximum masonry compressions were calculated for the two worst case walls for in-plane loads added to the out-of-plane face shell stresses computed in the response to Item 4(a). It was shown that the maximum compression did not exceed the ultimate capacity of the masonry face shell.

h. **ITEM 4(h)** Wall Attachments : The local and overall effects of attachments were considered and it was demonstrated that the connections had ample strength and were configured such that local failure modes would not occur.

The overall response to these detailed technical questions confirms that the assumptions on which the methodology was based provide a conservative estimate of the maximum wall response. It is considered that the cumulative effect of the conservatisms introduced to the various facets of the model would provide upper bound values of the overall wall deformations and for the detailed material stresses and strains.

Enclosure 2

Results of Energy Balance Evaluation of Masonry Walls

San Onofre Unit 1

Some of the steel reinforced concrete block walls at San Onofre Nuclear Generating Station, Unit 1 are expected to respond in the inelastic range under Design Basis Earthquake (DBE) loading. These walls have been subjected to a nonlinear time history analysis by Computech Engineering Services, Inc. The results of these analyses are reported in Volume 3 of the report Seismic Evaluation of Reinforced Concrete Masonry Walls, which was submitted to the NRC by letter dated January 11, 1982.

In addition to the above mentioned analysis, the masonry walls have also been analyzed utilizing the energy balance technique as outlined in Section 3.7.3.16.1 of the Balance of Plant Structures Seismic Reevaluation Critieria, which was submitted to the NRC by letter dated February 17, 1981. The results of this analysis are presented in Table 1 and Figure 1. For each masonry wall a range of ductilities is listed. The higher value represents the calculated ductility under DBE loading for the single section of wall having the most attached equipment. The lower value shown for each wall represents the calculated ductility for those sections of the wall having little or no attached equipment. Similar walls have been analyzed as a group. Therefore, the ductilities listed for each wall represent the range of required ductility between sections of that wall with little or no attached equipment and the one section of wall within the group having the most attached equipment.

Table 1:

Ductility Requirements of Masonry Walls Based on Energy Balance Technique.

WALL	LENGTH (ft.)	DUCTILITY REQUIRED
TB1A	40	3.6 - 4.6
TB1B	30	1.2 - 1.9
TB2	19	2.5 - 4.3
TB3	14	2.7 - 4.3
TB4	8	2.5 - 4.3
TB5	10	3.6 - 4.8
TB6	30	3.6 - 4.8
TB7A	40	3.6 - 4.6
TB7B	30	1.2 - 1.9
TB8	19	2.7 - 4.9
TB9	14	4.6 - 6.1
TB10	32	4.0 - 5.2
TB11	112	4.6 - 6.1
TB12	49	1.8 - 3.5
SB1A	21	2.4 - 2.7
SB1B	20	remains elastic
SB2	33	2.4 - 2.7
SB3	17	remains elastic
SB4	21	2.4 - 2.7
SB5	20	remains elastic
SB6	33	remains elastic
SB7	21	2.4 - 2.7
VB1	44	1.4 - 2.1
VB2	44	1.4 - 2.1
VB3	21	1.4 - 2.1
VB4	21	1.4 - 2.1

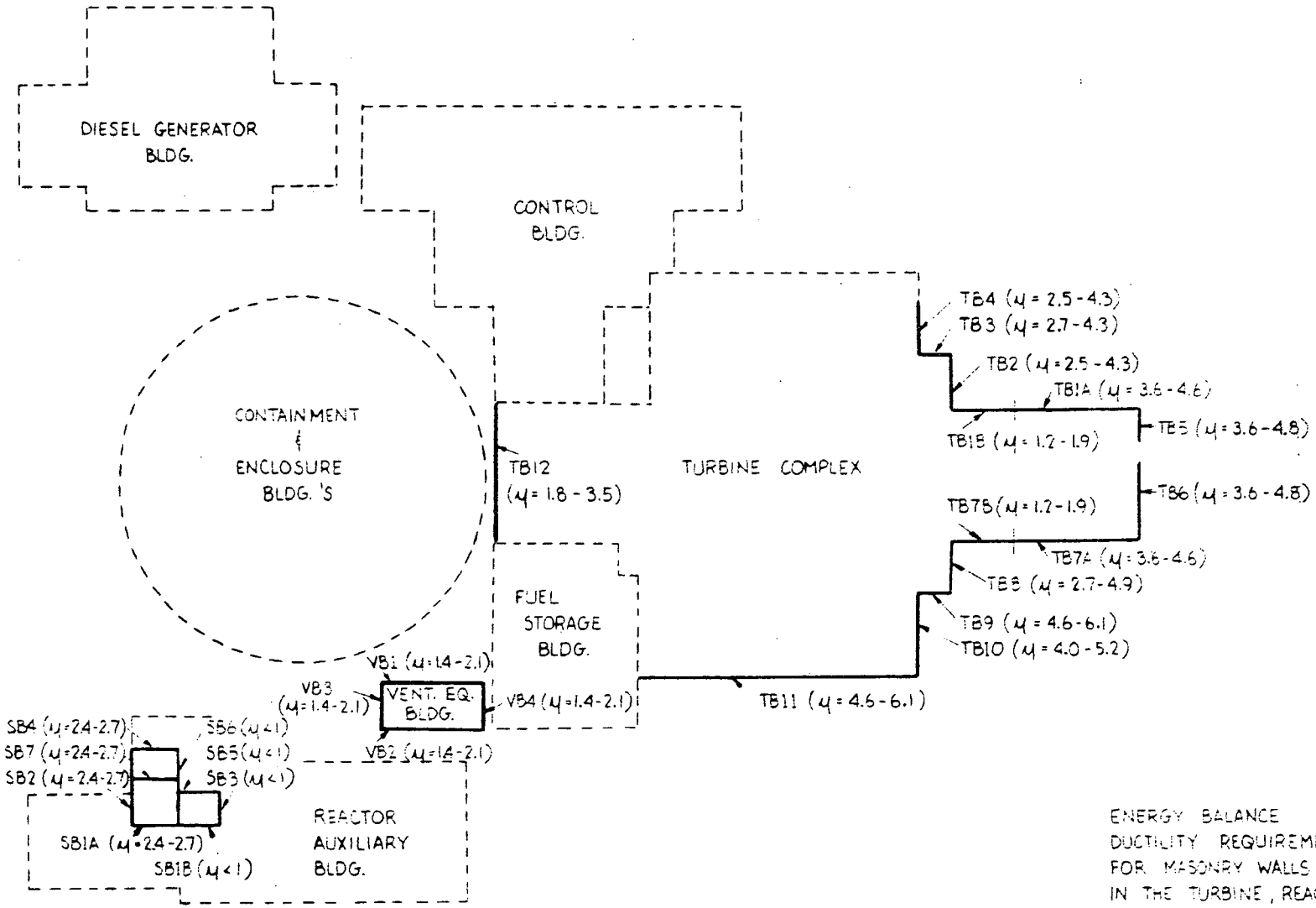

FIGURE 1

ENERGY BALANCE DUCTILITY REQUIREMENTS FOR MASONRY WALLS IN THE TURBINE, REACTOR AUXILIARY AND VENTILATION EQUIPMENT BUILDINGS